Fuel saving potential of a long haul heavy duty vehicle equipped with an electrical variable transmission

Ayoub Aroua, Walter Lhomme, Eduardo Redondo-Iglesias, Florian Verbelen

Fuel Saving Potential of a Long Haul Heavy Duty Vehicle equipped with an Electrical Variable Transmission

Ayoub Aroua[a,b], Walter Lhomme[a,*], Eduardo Redondo-Iglesias[c], Florian Verbelen[b,d]

[a] *Univ. Lille, Arts et Metiers Institute of Technology, Centrale Lille, Junia, ULR 2697 - L2EP, F-59000 Lille, France*
[b] *Department of Electromechanical, Systems and Metal Engineering, Ghent University, Belgium*
[c] *Univ. Lyon, IFSTTAR, AME, Eco7, F-69675 Lyon, France*
[d] *Flanders Make@UGent – core lab EEDT-MP, Belgium*

[*]Corresponding author: walter.lhomme@univ-lille.fr.

***Abstract*— The series-parallel architecture is the most interesting for hybrid electric vehicles, allowing the lowest fuel consumption. Unlike passenger cars, this architecture is not commercially available on the heavy-duty vehicles market. This is due to technical limitations associated with unsufficient load capability of the geartrain. To address this issue, new transmissions, such as the electrical variable transmission, have been developed. The novelty of this paper relies on the hybridization of a long-haul truck using the electrical variable transmission. This study aims to investigate the potential of using this new transmission for trucks. For that aim, fuel consumption benchmarking of three powertrain topologies is performed, considering: (a) a gearless topology; (b) a geared topology that uses one gearbox inserted between the engine and the mechanical input port of the electrical variable transmission; (c) a geared topology similar to the second one, but, with an additional multi-stage gearbox inserted to the mechanical output port of the electrical variable transmission. For a fair comparison between the different topologies, a bi-level optimization process has been used, incorporating the optimization of both components sizing and control. Results show that the fuel consumption of the gearless powertrain is higher than the engine-powered truck due to higher losses in the electrical variable transmission. While maximum fuel reduction of 14.2% was obtained by a geared topology that uses two gearboxes. Furthermore, emphasis is given to understand the effect of the powertrain component sizing on fuel consumption. Depending on the defined sizing, a possible fuel reduction is achieved from 3.3% to 14.2% for the two geared topologies. The reduction of CO_2 emissions is found to be proportional to the fuel savings. Considering a long-haul mission, the last findings prove that the electrical variable transmission exhibits potential to reduce fuel consumption, if an adequate powertrain topology and its sizing are well defined.**

Keywords*— *Powertrain design, Series-parallel architecture, Dedicated Hybrid Transmission, Scaling Factors, Bi-level optimization approach, Energy Management Strategy, Dynamic Programming.

LIST OF ABBREVIATIONS

AMT	Automated Manuel Transmission
BSFC	Brake Specific Fuel Consumption
CO_2	Carbon dioxide
DP	Dynamic Programming
EMR	Energetic Macroscopic Representation
EMS	Energy Management Strategy
EVT	Electrical Variable Transmission
HDV	Heavy Duty Vehicle
HEV	Hybrid Electric Vehicle
ICE	Internal Combustion Engine

IR	Inner Rotor
LUT	Look Up Table
OCV	Open Circuit Voltage
OR	Outer Rotor
PA	Power Adaptation element (EMR element)
PM	Permanent Magnet
PMSM	Permanent Magnet Synchronous Machine
SoC	State of Charge
VECTO	Vehicle Energy Consumption Calculation Tool

1. Introduction

Over the last decades, the efficiency of Heavy-Duty Vehicles (HDV) in Europe has not been increased, resulting in no significant emissions reductions [1]. This due essentially to the absence of addressing legislation to regulate and monitor the emissions of road freight transportation. In 2018, the European Commission of the European Union has set up its first-ever carbon dioxide (CO_2) standard for new HDV [2]. This latter will have to contribute towards a CO_2 reduction of 15% by 2025 and 30% by 2030, compared to 2019 baselines. With this new regulation, the European Union is the sixth nation to impose mandatory CO_2 standards for HDV, after the United States, Canada, China, Japan, and India [3]. In the first phase of the standard, strict certification measures have been set up for new HDV. This certification procedure rests on reporting and monitoring CO_2 emissions and fuel consumption. To do so, a simulation tool called VECTO (Vehicle Energy Consumption Calculation Tool) has been developed for Internal Combustion Engine (ICE) based-HDV [4]. This tool has a good fuel consumption calculation accuracy of $\pm$ 3.5% compared to on-road tests performed on real trucks [5].

While to ensure that the long-term CO_2 reduction objectives will be met, manufacturers and stakeholders will need to introduce new efficient technological solutions. The new standard leaves an open policy to choose suitable solutions, which enables a shift towards low-emission mobility. Measures and solutions, as described in [6,7], could help to achieve CO_2 mitigation and can be summarized as follows:

- Usage optimization: connectivity of roads using intelligent transport networks and automated driving systems exhibit potential to reduce fuel consumption, such as truck platooning and intelligent eco-driving guidance.
- Efficiency improvement: an efficiency increase can be made possible by improving the aerodynamic performances of the vehicle, i.e. reducing the air drag coefficient by innovating new cabin and trailer designs. Moreover, low rolling resistance tires, engine efficiency, and recovering heat waste can effectively contribute to reducing fuel consumption.
- The adaptation of new energy carriers: liquefied natural gas and liquefied biogas are low-emission fuel alternatives for decarbonizing the road freight sector. Due to its chemical

composition, gas-based technologies lead to lower CO_2 emissions compared to diesel vehicles. Some truckmakers are promoting liquefied natural gas-based technologies, as the way forward to meeting the CO_2 emission targets in the short and medium term. In the same context, hydrogen seems a promising solution for HDV thanks to its energy density, which offers a high range. Hydrogen can be used in fuel cells to generate electricity for the electrical drive. A neutral well-to-wheel carbon balance can be achieved using green hydrogen produced from renewable energy, which helps to achieve the zero-emission objective. However, obstacles such as refueling and delivery infrastructure, high production costs, storage, and transportation are challenging the expansion of these new energy carriers.

- Powertrains electrification: truck manufacturers are increasingly believing in this option. Hybrid, battery, and fuel cell vehicles hold potential for achieving low and zero-emission mobility objectives. This type of vehicle can significantly reduce the CO_2 emissions in the well-to-wheel balance.

The scope of this paper is restricted to focusing on the powertrain hybridization with an ICE and a battery. Hybrid Electric Vehicles (HEV) provide a solution to improve fuel economy and thereby reduce emissions to cope to a certain extent with the new legislation. Three main architectures for deriving an HEV powertrain are possible: a series architecture, a parallel architecture, and a series-parallel architecture [8]. For light-duty vehicles, the series-parallel architecture, such as the Toyota hybrid system, is the most interesting. This architecture enables more degrees of freedom, resulting in the lowest fuel consumption compared to the series and parallel architectures [9]. The key core element of the series-parallel architecture is a power split device. This latter can be classified into two categories, namely electromechanical and electromagnetic. Most passenger cars with series-parallel configuration use an electromechanical power split device, which consists of two electrical drives (two electric machines with their power electronic converters) and a planetary geartrain. For heavy-duty applications, the series-parallel architecture is not available yet on a large scale. The series and parallel architectures are more prevalent [10-11]. This due to mechanical constraints related to the planetary geartrain. A single planetary geartrain would not satisfy the torque requirement of heavy-duty applications because of some constraints as weight and size. To counter this problem, a lot of research work focuses on technical solutions for HDV series-parallel architecture. Some studies suggest using cascaded planetary gears with clutches [12-14] or a compound planetary geartrain such as the Ravigneaux geartrain [15]. The latest solutions are interesting and feasible, but on the other hand, mechanical losses and design complexity will increase considerably.

Another alternative to overcome these technical issues, for series-parallel architecture, would be to consider an electromagnetic power split device, namely the Electrical Variable Transmission (EVT) [16]. The idea of the EVT consists of replacing the Toyota hybrid system with one compact electromagnetic component that combines the functionality of the planetary gearbox and the two

electrical machines. It is composed of a wound inner rotor supplied by slip rings, an outer rotor with Permanents Magnets (PM) or squirrel cage, a stator, and power electronics converters. The power coming from the ICE and the battery will be split through an electromagnetic path instead of an electro-mechanical path. Electromagnetic interaction between both rotors will occur, enabling to transmit a part of the power coming from the engine directly to the final drive without any mechanical connection like planetary geartrain. The remaining power can be stored in the battery or transmitted to the outer rotor through the stator, depending on the required traction power. The main advantages of an EVT over the mechanical transmission are the reduced maintenance requirements, lower losses, and a high torque load capacity, making it suitable for HDV.

A variety of EVT topologies were proposed in literature for automotive applications. PM versions are more interesting because of a higher torque density and efficiency. Three main designs of PM-EVT can be found: two PM layers [17], a single PM layer [18], and hybrid excited EVT [19]. The last version has a thin outer rotor that combines a single PM layer with a DC-field winding, hence the hybrid excited name. Among these versions, the hybrid excited EVT has lower losses [20]. This is a result of strong magnetic coupling between the EVT subcomponents because of the thickness of the outer rotor. Consequently, the performance will depend on this magnetic coupling, which gives more degrees of freedom to generate the torque more effectively. The DC field winding adds also another degree of freedom to manipulate the stator flux, allowing further optimization of the losses. Recent research [21] has shown the added value of the hybrid excited EVT for a passenger car in terms of fuel savings. A comparison with the Toyota hybrid system for several driving cycles showed that the EVT enables on average a possible fuel economy of 4.75%.

The main novelty of this paper lies in the hybridization of a long-haul conventional truck, using the hybrid excited EVT. Some literature studies have focused on the hybridization of different vehicle classes using the EVT, e.g. passenger cars [21], medium-duty trucks [22], and city busses [23]. However, no study to date has been conducted on the hybridization of a long-haul engine-powered truck using an EVT. One of the interesting questions addressed in this paper is the potential of fuel reduction of a long-haul truck, which is driven most of the time on highways at a steady speed. The presented work aims then to investigate the benefits of such a hybrid powertrain in terms of fuel savings, compared to a reference conventional long haul HDV. The key contributions of this work are summarized as follows:

- a comparison between a long-haul engine-powered truck and hybrid truck equipped with an EVT, based on an accurate dataset, to quantify the fuel savings;
- a benchmark analysis of three different EVT powertrain topologies with a focus on understanding the impact of the topology choice, the components sizing and their interrelation on the fuel consumption;

Regarding the first contribution, the starting point of this paper is a reference engine-powered truck from VECTO. Although this tool is capable of simulating many types of engine-powered trucks, it cannot yet simulate hybrid powertrains. According to [11], the next version of VECTO will include

series and parallel hybrid trucks, but it is not intended to integrate the series-parallel architecture. Hence, a simulation tool in Matlab-Simulink® is developed to hybridize the reference truck and assess the energy savings. This tool needs to have accurate fuel consumption calculations as VECTO. To this end, the dataset of the reference truck has been extracted from VECTO database and reused to simulate the reference truck with the developed tool to check its fuel calculations. Regarding the EVT, an existing prototype has been characterized on a test rig [20]. It is worth noting that the actual EVT prototype has been designed for a hybrid passenger car. To upscale the prototype design, scaling laws are used to meet the requirement of an HDV application. These scaling laws have been firstly derived by [24] for a Permanent Magnet Synchronous Machine (PMSM) and validated for PM-EVT by [25]. These scaling laws enable to adaptively, rapidly, and precisely re-calculate a new EVT design for various vehicle classes without re-doing the finite element calculation for each new design. Such a theory is based on three scaling factors, which are axial, radial, and rewinding. These factors allow scaling the machine properties (e.g. voltage, torque, power, losses…) along with the machine parameters (e.g. resistance, inductance, inertia…).

Regarding the second contribution, knowledge of the impact of topological choices of an EVT powertrain is limited, in particular for heavy-duty trucks, which is indispensable for assessing the full potential of these types of vehicles. Three EVT-based powertrain topologies will be investigated in this paper, considering one gearless topology, two geared topologies by adding gearboxes in different locations of the powertrain. The fuel consumption of these powertrains will be benchmarked with the scope of highlighting the impact of the sizing of the powertrain components and the topological design choices. For each topology, a bi-level optimization is performed using the existing optimization methods, by examining both the plant design and its control due to a strong coupling between the two [26]. It is worth emphasizing that it is not the goal of this paper to improve the existing optimization methods that have been used for system-level optimization or to develop a new methodology. The main contribution is the comparison itself and the in-depth analysis of powertrain design choices, which has not yet been performed for EVT based-powertrains. In this context, prior research works have focused on no more than one design level (e.g. control) or two levels at maximum (e.g., sizing and control). However, to define an optimal powertrain design, the system-level design with its all sub-levels namely topology, component technologies, sizing, and control needs to be investigated within a coupled optimization framework [27]. The energy consumption will therefore depend on the interaction between these powertrain design levels [28]. These design layers are interconnected and will influence one another, which can lead to sub-optimal solutions if investigated separately [29]. On the other hand, considering the four design layers results in a multi-level coupled optimization problem, which implies a wide range of functional evaluations that increase with the number of design parameters. The first research works such as [30] have focused on the optimization of the control level, also known as Energy Management Strategy (EMS), using Dynamic Programming (DP) to investigate the fuel consumption of an EVT based-powertrain. DP is typically used in literature to optimize the control and benchmark the energy

consumption of different electrified vehicles. This method determines the optimal control policy by computing all possible control inputs at each time step of a given driving cycle [31]. Further research has incorporated the EVT powertrain sizing in the optimization problem along with the control optimization [21]. However, the authors of the last-mentioned paper have only optimized the EVT size and overlooked the remaining powertrain components sizing. Ma *et al* [32] have developed a more general co-design optimization, taking into account all the powertrain subcomponents sizing. Although the last-mentioned papers tackled the design problem of EVT powertrains by optimizing component sizing and control, the topology of the powertrain is kept fixed. This means that the system-level design optimization in its entirety with its various levels has not yet been extensively studied.

The rest of the paper is structured as follows. Section 2 presents the European HDV simulation tool VECTO, the reference engine-powered long-haul truck and its powertrain modelling, and the driving cycle. In Section 3, three powertrain topologies based on EVT will be presented and studied. This section details the modelling of each topology. Section 4 is devoted to introducing the bi-level optimization framework for the three EVT powertrains. The performances of the studied EVT powertrain configuration in terms of fuel savings are presented and discussed in Section 5. Finally, the conclusion and the perspectives are reported in Section 6.

2. Engine-powered long-haul vehicle

This section aims to benchmark the fuel consumption of the reference engine-powered vehicle using the developed tool in Matlab-Simulink®. The first part of this section introduces the VECTO simulation tool, the reference truck, and the studied driving cycle. Secondly, the models of the powertrain sub-components and their interactions are detailed using EMR. Afterward, an optimal gear shifting strategy is developed, using DP, to find the optimal fuel consumption. Finally, the last subsection is dedicated to the validation of the results obtained from the Matlab simulation tool, by performing a comparison with VECTO.

2.1. VECTO & reference truck

A chassis dynamometer testing is generally performed to assess the emission of light-duty vehicles. This procedure consists of putting the vehicle on a testbed and measures its efficiency during a normalized test cycle. This methodology is complex and not possible for HDV because of the high testing cost and the high customizability. For these reasons, the European Commission has developed VECTO. This tool determines the fuel consumption and CO_2 emissions of the vehicle based on components data, following a backward simulation approach (wheel-to-engine approach). In this way, VECTO can determine the fuel consumption of a wide variety of HDV, for multiple different mission profiles. Since VECTO's vehicles data are certified and accurate, they are being accordingly extracted to build a Matlab-Simulink® simulation program. VECTO divides trucks into 18 groups based on the axle configuration (4x2, 6x2, 8x2, etc.), the body configuration (rigid or tractor), and the gross vehicle

weight [33]. As reported in [34], 79% of the overall CO_2 emissions of trucks are originated from groups 4, 5, 9, and 10. Therefore, it is decided to focus on the electrification of a long-haul truck, belonging to group 9. The powertrain of the reference truck consists of an ICE, a clutch, a 12-speed Automated Manual Transmission (AMT) gearbox, and the final drive, as illustrated in Fig. 1. The main parameters of the truck are summarized in Table 1.

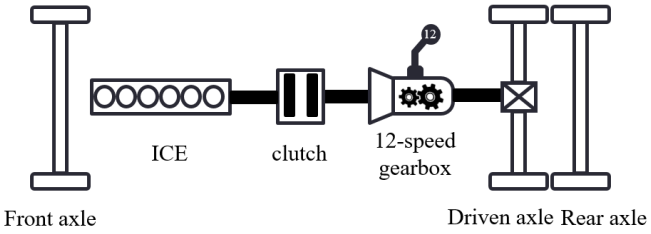

Fig. 1: Reference ICE based HDV powertrain

Table 1: Reference truck parameters

Truck group	**9**
Mission profile	Long haul
Axle configuration	**6x2**, i.e. 3 axles in which the only one of the rear axles is driven by the gearbox.
Total vehicle mass [kg]	**36200**
Transmission	**12-speed Automated Manual Transmission (AMT)**
Possible gear ratio (12-speed AMT)	{14.93, 11.64, 9, 7, 5.64, 4.4, 3.39, 2.65, 2, 1.6, 1.28, 1}
Auxiliaries average power	**4.4 kW**, including electric and pneumatic systems, steering pump, and fan cooling circuit power demands

2.2. Reference driving cycle

To calculate the fuel consumption, the VECTO's long-haul driving cycle is used. This cycle is a shortened version of a long-haul driving cycle (around 80 minutes), developed to limit simulation time. However, it keeps the typical long-haul driving proprieties, i.e. this cycle is dominated by highway driving with low dynamics and a constant speed. The grade profile is also defined in this cycle. The speed and grade profile are illustrated in Fig.2. The fuel consumption over this cycle, obtained via a backward simulation carried out by VECTO, is equal to 37.38 l/100km. This consumption results in 971g/km of CO_2 emissions for the driving cycle under consideration.

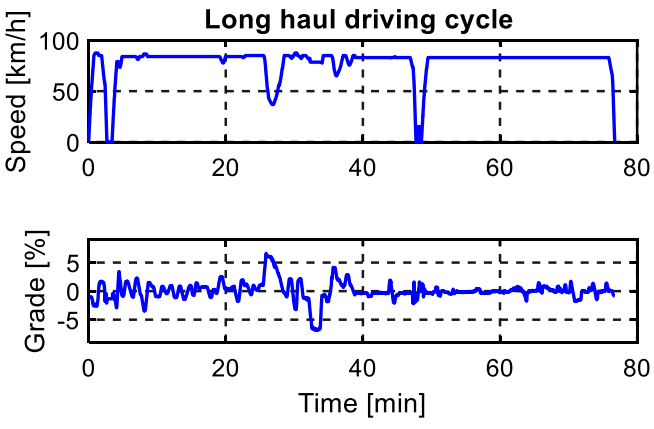

Fig.2: VECTO long haul driving cycle

2.3. Modelling and EMR- backward oriented description of the reference truck

This subsection details the models of the powertrain sub-components. As VECTO uses a backward approach and for fair comparison reasons, the Energetic Macroscopic Representation (EMR)-oriented backward description is used throughout this work to organize and describe the vehicle model [35]. EMR is a graphical formalism based on a systemic approach, allowing to have a clear and comprehensible understanding of the power flows in a system and the interaction between its components [36]. EMR translates the models of each component into graphical elements that describe its function in the system: source of energy (oval), accumulation of energy (crossed rectangle), conversion of energy (square or circle), distribution of energy (overlapped square or circle), and power adaptation (square with a mathematical comparison sign inside). EMR methodology basically provides a forward description (engine-to-wheel approach) of a multi-domain system, such as electrified vehicles, for control purposes [37,38]. In recent studies, this formalism has been used in off-line optimization problems, which are based on a backward approach, for electrified vehicles [21,32,39]. To this end, the forward description has been transformed into a backward description. A quasi-static model of the reference truck powertrain has been developed to carry out an energetic study. This type of model enables a good accuracy of the overall fuel consumption. The EMR-oriented backward description of the reference truck is shown in Fig. 3. Table 2 provides an overview of EMR-oriented backward approach pictograms. The oval pictograms describe four mechanical sources: one for the engine (ICE in Fig. 3), one for the environment (Env.), one equivalent mechanical source for the braking system (Brakes), and one for the auxiliaries (Aux.). The gearbox, differential, and wheel are described by square pictograms to perform a mono-domain conversion of the power, in this case mechanical to mechanical. The overlapped square represents a distribution of the power coming from the engine to the traction part and the auxiliaries. The accumulation element, used to describe the chassis, emphasizes the fact that energy is stored inside. The dynamics of the vehicle are taken into account as the acceleration is known beforehand and described by the accumulation element. Finally, the EMS pictogram highlights the degrees of freedom for the control: k_{gb}: the desired gear ratio and k_{d}: the braking criteria. Notice that the product between variables of two interconnected pictograms gives instantaneous power. Additionally, it should be noted that each pictogram is linked with its modelling equation The models of the powertrain sub-components are detailed in the following subsections.

a. Environment

The environment is considered as a source of a resistive force F_{res}, which depends on several parameters as shown in eq. (1). Due to the backward approach, the imposed driving cycle speed v_{veh}^{*} is assumed equal to the achieved speed v_{veh} , eq. (2).

$$F_{res} = \frac{1}{2}\rho_{\mathrm{air}}\left[C_{\mathrm{d}}.A(v_{\mathrm{veh}}){v_{\mathrm{veh}}}^{2} + M_{\mathrm{veh}}\ g\ \sin\left(\delta_{\mathrm{grade}}\right) + k_{\mathrm{rr}}\ M_{\mathrm{veh}}\ g\ \cos\left(\delta_{\mathrm{grade}}\right)\right] \quad (1)$$

$$v_{\mathrm{veh}} = v_{\mathrm{veh}}^{*} \quad (2)$$

where ρ_{air} is the air density, C_{d} is the air drag coefficient, A is the frontal area, M_{veh} is the total mass of the vehicle, g is the gravitational acceleration δ_{grade} is the angle of incline and k_{rr} is the rolling resistance coefficient.

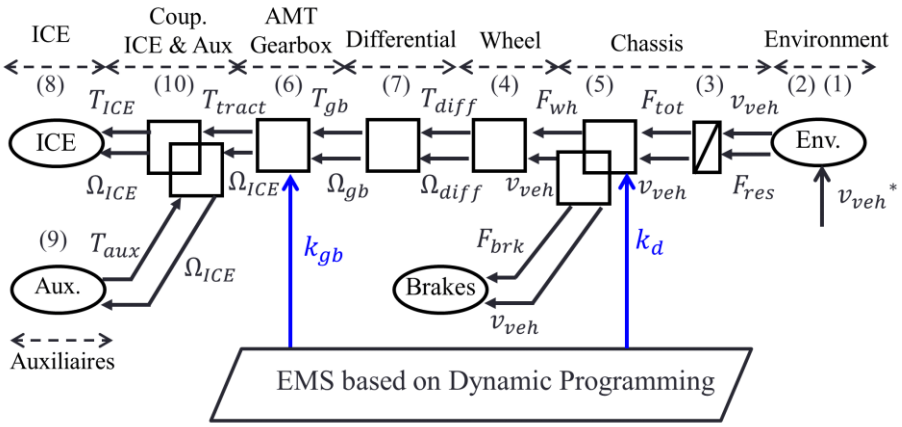

Fig. 3: Engine-powered truck and its EMR- oriented backward approach

Table 2:Pictograms of Energetic Macroscopic Representation (EMR) oriented backward approach

	Source Element (energy source)		Accumulation element (energy storage)		Mono-domain conversion element
	Multi-domain conversion element		Mono-domain coupling element (energy distribution)		Power adaptation element (less than)
	Power adaptation element (greater than)		Energy Management Strategy		

b. Chassis

The chassis represents the principal dynamic of the system. In the backward approach, the acceleration of the truck is known beforehand. The traction force F_{tot} is then given by applying the second law of Newton, based on eq. (3).

$$F_{\mathrm{tot}} = M_{\mathrm{veh}} \frac{d\, v_{\mathrm{veh}}}{dt} + F_{\mathrm{res}} \qquad (3)$$

c. Wheels & Mechanical brakes

The road-tire contact is neglected in this study and the model of a single equivalent wheel has been adopted. The wheel converts an angular speed Ω_{diff} to a linear speed v_{veh} , see eq. (4). The force developed at the wheels F_{wh} and the braking force F_{brk} are defined through a braking distribution criteria k_{d} , according to eq. (5).

$$\begin{cases} F_{\mathrm{wh}} = \dfrac{T_{\mathrm{diff}}}{r_{\mathrm{wh}}} \\ \Omega_{\mathrm{diff}} = \dfrac{v_{\mathrm{veh}}}{r_{\mathrm{wh}}} \end{cases} \quad (4)$$

$$\begin{cases} F_{\mathrm{wh}} = (1 - k_{\mathrm{d}})\, F_{\mathrm{tot}} \\ F_{\mathrm{brk}} = k_{\mathrm{d}}\, F_{\mathrm{tot}} \\ 0 \leq k_{\mathrm{d}} \leq 1 \end{cases} \quad (5)$$

d. AMT gearbox & differential

Efficiency maps extracted from VECTO are being used to define the efficiency of the gearbox η_{gb} and the differential η_{diff}, according to the operating points. The reference truck uses a 12-speed AMT gearbox. The ratio of the gearbox k_{gb} is considered as an input signal command and it can take 12 discrete values between 1 and 14.93 (see Table 1). The torque and angular speed relationships of the transmission part are given by eq. (6) and (7).

$$\begin{cases} T_{\mathrm{gb}} = k_{\mathrm{gb}}\, T_{\mathrm{tract}}\, \eta_{\mathrm{gb}} \\ \Omega_{ICE} = k_{gb}\, \Omega_{gb} \end{cases} \quad (6)$$

$$\begin{cases} T_{\mathrm{diff}} = k_{\mathrm{diff}}\, T_{\mathrm{gb}}\, \eta_{\mathrm{diff}} \\ \Omega_{\mathrm{gb}} = k_{\mathrm{diff}}\, \Omega_{\mathrm{diff}} \end{cases} \quad (7)$$

e. Clutch

As this study focuses solely on energetic aspects, clutches can be neglected for simplicity reasons [40]. However, the idle speed of the ICE is taken into account to avoid divergence in fuel consumption.

f. Engine

A static model of the ICE is used, i.e. the dynamics are ignored. The achieved operating points of the ICE (torque T_{ICE} and angular speed Ω_{ICE}) are then used to determine its instantaneous Brake Specific Fuel Consumption (BSFC) through an engine map extracted from VECTO, see eq. (8). Total CO_2 emissions are calculated following the method proposed in VECTO [41], as the product of the mass of fuel m_{fuel} consumed during the driving and a constant emission factor k that depends on the fuel type.

$$\begin{cases} BSFC = f(T_{ICE}, \Omega_{ICE}) \\ CO_2 = k\, m_{\mathrm{fuel}} \end{cases} \quad (8)$$

g. Auxiliaries

Average power consumption of 4.4 kW is considered for the auxiliaries (see Table 1). Note that this value has been extracted from VECTO. For the conventional truck, the auxiliaries are considered as a load torque T_{aux} and the model is given by eq. (9). The engine torque T_{ICE} is therefore the result of the sum of the traction torque T_{tract} and T_{aux} , eq. (10).

$$T_{\mathrm{aux}} = \frac{P_{\mathrm{aux}}}{\Omega_{\mathrm{ICE}}} \quad (9)$$

$$T_{\mathrm{ICE}} = T_{\mathrm{tract}} + T_{\mathrm{aux}} \quad (10)$$

2.4. Energy Management Strategy

One of the strengths of the EMR methodology is to highlight distribution criteria and output signals defined by the global control or the so-called Energy Management Strategy (EMS). This level of control must be carried out according to the defined objectives to minimize a cost function, for example reducing the fuel consumption in this study. Thereby, the outputs defined by the EMS act on the local control to reduce this cost. Herein, two output signals (k_{d} and k_{gb}) are determined by the EMS for the conventional truck to manage the braking and the gear shifting respectively. Note that VECTO uses a rule-based strategy based on a shifting schedule [42]. As it was not possible to access this strategy and extract its algorithm, DP is chosen to benchmark the fuel consumption. DP is an optimal offline method. It is widely used to optimize the EMS of conventional and electrified vehicles based on a pre-specified driving cycle [43]. In this sense, DP is used to define an optimal gear shifting strategy, which minimizes the fuel cost function *J* over the long haul driving cycle. This cost function *J* is the sum of the state transfer costs *L* (cost between two-step times *k* and *k+1*). In this case, the state transfer cost *L* is the fuel mass flow $\dot{m}_{\mathrm{fuel}}$.

$$J = \sum_{k=1}^{N} L(x(k), u(k), k) = \dot{m}_{\mathrm{fuel}}(x(k), u(k), k) \quad (11)$$

In contrast with VECTO, no engine braking is considered as it has no impact on fuel consumption. Broadly speaking, engine braking in heavy-duty vehicles is used to alleviate and support the braking system and help to reduce the wear of friction brakes. From an energetic point of view, this assumption does not impact fuel consumption since no braking energy recovery is possible in engine-powered vehicles, and this braking energy is dissipated in the form of heat. Furthermore, this choice allows simplifying the optimization problem. Under the above assumption, k_{d} can be seen then as a boolean variable (1 for braking and 0 if no braking), which is defined by a simple rule inserted in the code to save computational time. Concerning the gear shifting, the next gear can be expressed as a function of a current gear number $n_{\mathrm{gb}}(k)$ and a shift command $u_{\mathrm{gb}}(k)$ as shown in (12). Consequently, the gear ratio k_{gb} can be written as eq. (13). The state variable $x(k)$ is herein the current gear number $n_{\mathrm{gb}}(k)$ [44], which can take any integer between 1 and 12 (12-speed AMT, see Table 1), and the control variable $u(k)$ is the shift command $u_{\mathrm{gb}}(k)$. The gear shifting dynamic is given by eq. (14).

$$n_{\mathrm{gb}}(k+1) = n_{\mathrm{gb}}(k) + u_{\mathrm{gb}}(k) \quad (12)$$

$$k_{\mathrm{gb}}(k) = ratio\left[n_{\mathrm{gb}}(k) + u_{\mathrm{gb}}(k) \right] \quad (13)$$

$$x(k+1) = n_{\mathrm{gb}}(k+1) = \begin{cases} 1, & n_{\mathrm{gb}}(k) + u_{\mathrm{gb}}(k) < 1 \\ 12, & n_{\mathrm{gb}}(k) + u_{\mathrm{gb}}(k) > 12 \\ n_{\mathrm{gb}}(k) + u_{\mathrm{gb}}(k), & \text{otherwise} \end{cases} \quad (14)$$

To prevent a large variation in the shifting process, the shift command has been fixed to vary within the interval [-4,4] [45]. It means the maximum gear skipping is 4 gears, if the resulting gear is

feasible. Finally, it should be noted that the cost function, eq. (11), is subjected to some constraints related to the engine speed and torque, as described by eq. (15).

$$\begin{cases} \Omega_{ICE-min} \leq \Omega_{ICE}(k) \leq \Omega_{ICE-max} \\ T_{ICE-min} \leq T_{ICE}(k) \leq T_{ICE-max} \end{cases} \quad (15)$$

2.5. Validation of the engine-powered truck model

The gear shifting proposed by DP is illustrated in Fig. 4.a. The simulation results show the engine limitations (torque and speed Fig. 4.b) are respected. It is also clearly seen that most of the ICE setpoints occupy a low BSFC area, which is equivalent to higher engine efficiency. The comparison made in Fig. 5 shows that there is a difference of 2% between the fuel consumption found in VECTO and DP-based backward EMR approach. This confirms that the simulation of the reference vehicle is sufficiently accurate. This slight difference can be explained by the fact that the proposed gear shifting is a result of optimal solutions, however, on the other hand, VECTO uses a rule-based strategy that does not guarantee optimal consumption. Henceforth, the fuel consumption found by DP will be considered as the reference to perform the comparison with the EVT-based HDV.

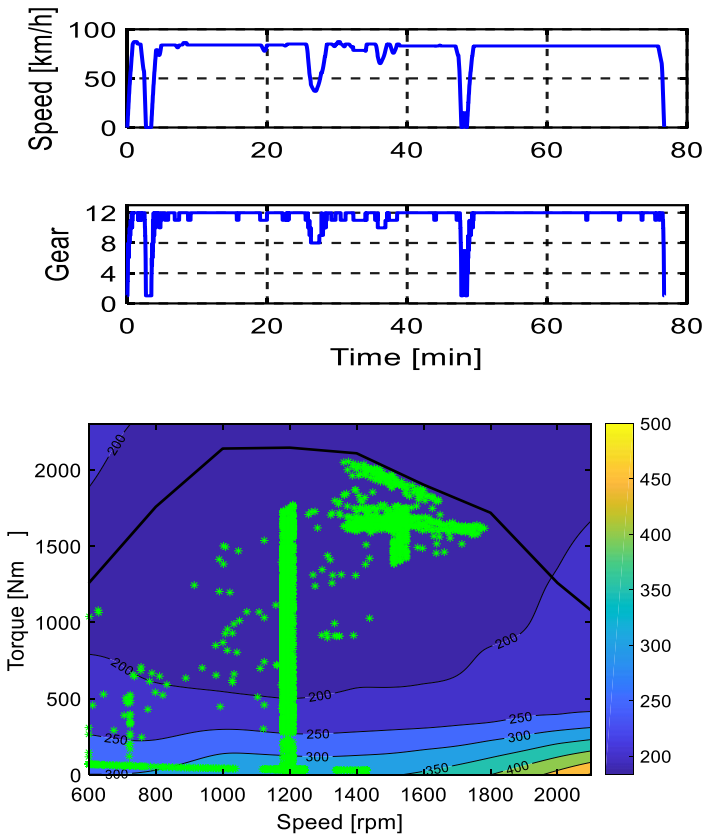

Fig. 4: Dynamic programming results for the reference truck: (a) Gear shifting result, (b) Engine operating points: Brake specific fuel consumption [g/kWh] as a function of engine speed and torque

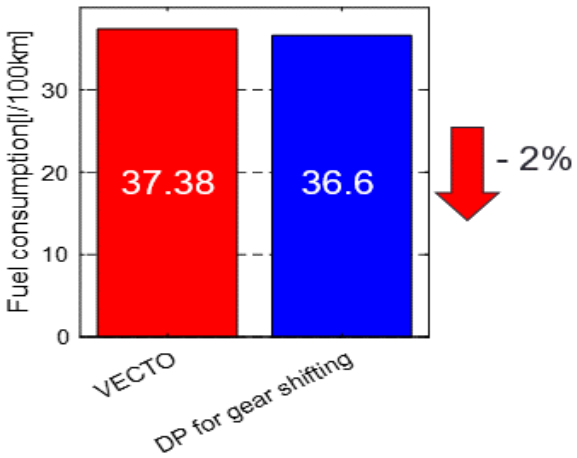

Fig. 5: Fuel consumption results of both VECTO and dynamic programming

3. EVT based Heavy-Duty Vehicle

The powertrain of the EVT-based HDV can be conceived in several configurations. The most frequently used EVT powertrain in literature is a gearless configuration, i.e. it does not use any gearbox [21,22,30]. Other options can be considered, such as adding mechanical gearboxes to the mechanical input port or the output port of the EVT or both of them. For example, an EVT powertrain with a reduction gearbox inserted on the engine side is suggested by [46,47]. Other studies addressed the benefits of adding a 2-speed gearbox to the final drive of battery-electric heavy-duty trucks [48,49]. According to the latest mentioned research, this solution enables to improve the overall energy consumption and reduce the electrical machine size. Despite the advantage of the 2-speed gearbox in electrified powertrains, this latter is not discussed in literature for EVT powertrains. In this paper, a gearless topology and two geared topologies are investigated. This section presents these topologies and deals with their modelling. At the end of this section, particular attention is given to the explanation of the EVT scaling process and the structuration of the scaled model using the EMR methodology.

3.1. Presentation of the three studied topologies

As a reminder, the double excited EVT consists of an Outer Rotor (OR), an Inner Rotor (IR), a stator, and three power electronics converters. The first powertrain configuration is a gearless EVT powertrain, which is composed of an ICE connected to the IR, a battery connected to the power electronics converters, an OR connected to the final drive. The battery can exchange energy with the stator and the OR through two inverters and one chopper is used for the DC field winding. This topology is called further "**Topology A"** (Fig. 6.a). A second EVT powertrain is studied using a reduction gearbox between the ICE and the IR. This latter is named **"Topology B"** (Fig. 6.b). Finally, a second geared topology is investigated using a reduction gearbox inserted between the ICE and the IR and a two-speed gearbox connected to the OR and the final drive. The last-mentioned topology is hereinafter referred as **"Topology C"** (Fig. 6.c).

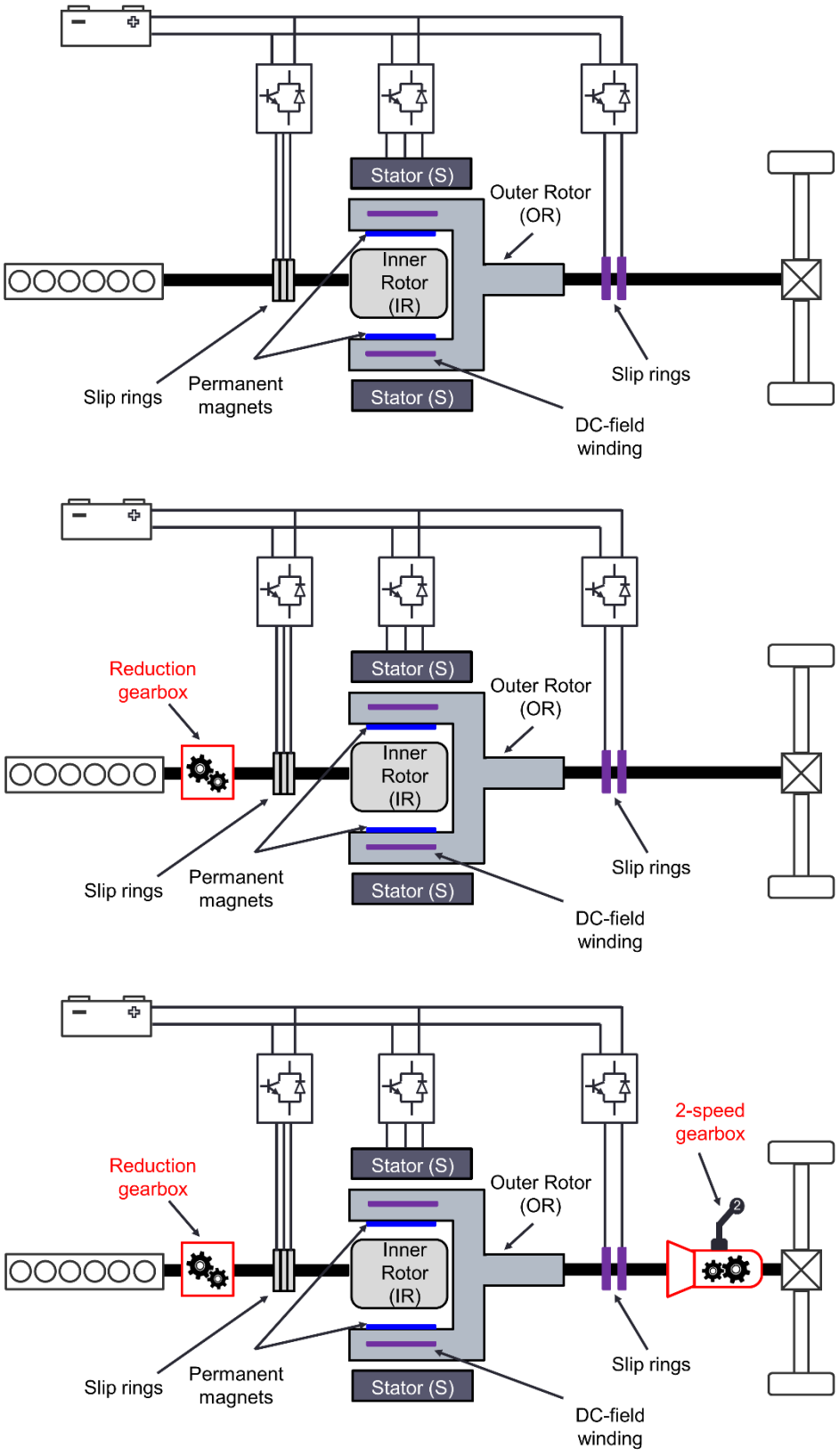

*Fig. 6: Studied powertrain topologies: a) Topology **A** – Gearless EVT powertrain topology, (b) Topology **B** – Geared EVT powertrain with a reduction gearbox, (c) Topology **C** – Geared EVT powertrain with both reduction gearbox and 2-speed gearbox; For simplicity, only the driven axle is represented.*

3.2. Modelling and EMR- oriented backward approach of the studied EVT powertrains

This subsection deals with the modelling and the description of the three studied topologies. Note that the models of common components compared to the ICE-based HDV (ICE, chassis, etc..) and their graphical descriptions are detailed in Section 2.3. Herein, a unified EMR-oriented backward description is proposed for the three studied powertrain topologies, as illustrated in Fig. 7. Recall that, the pictograms of the EMR-oriented backward are presented in Table 2. Compared to Fig. 3, an electrical source for the battery is added (Bat in Fig. 7). The power electronics converters and the additional gearboxes are described by square pictograms to perform mono-domain power conversions, electrical to electrical, and mechanical to mechanical respectively. The reference EVT is described with a multi-domain conversion element (circle in Fig. 7), which converts electrical power to mechanical power. More details Two power adaptations are used to enhance the fact that the reference EVT is scaled to fulfill the requirements of a heavy-duty truck. An underbar is used for the EVT variables to highlight the fact that some variables are grouped in an array: two torques and two speeds and five voltages and currents for both inner and outer rotors. A decoupling pictogram is used to indicate that there is an exchange of energy between the EVT, the engine, and the drivetrain of the truck. Further details on the models are presented in the subsequent subsections.

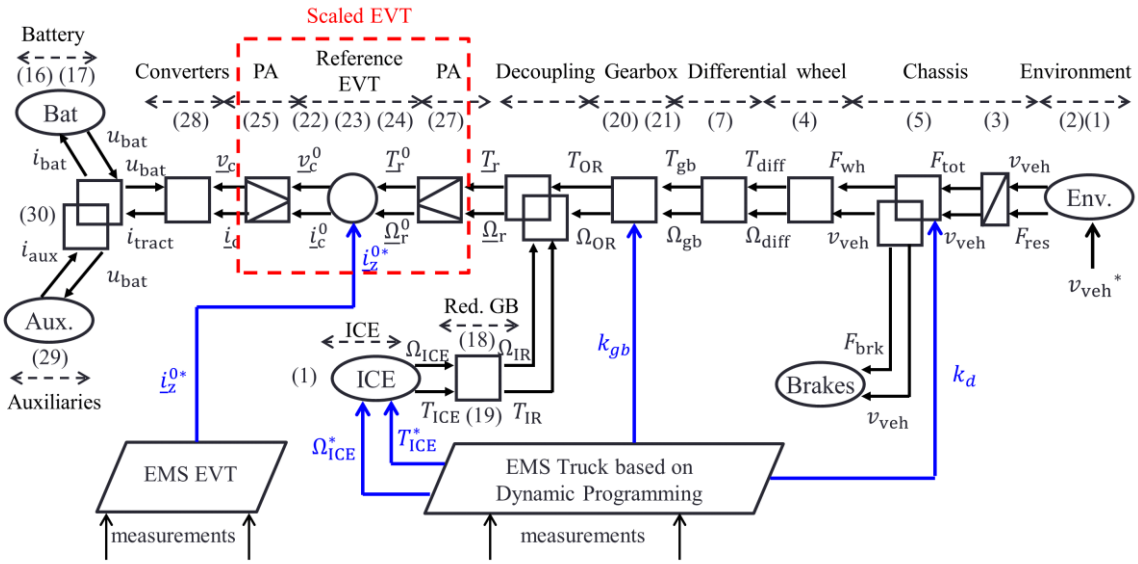

Fig. 7: EMR- oriented backward of the three proposed EVT powertrain topologies

a. Battery

A Li-ion battery ($LiFePO_4$) is used in this study. Lithium-ion batteries have a higher energy density and efficiency than other technologies, such as Lead-acid or NiMH. The battery has been characterized based on experimental tests, performed at the French transport laboratory LTE-IFSTTAR [50]. The model used in this study is a basic electrical model, i.e. Open Circuit Voltage (OCV) model with an internal resistance [51]. The OCV voltage and the internal resistance r_{bat} are non-linear functions of the battery State of Charge SoC_{bat} as described by eq. (16) and (17). By convention i_{bat} is positive, when discharging the battery.

$$u_{\mathrm{bat}} = u_{\mathrm{OCV}}(SoC_{\mathrm{bat}}) - r_{\mathrm{bat}}(SoC_{\mathrm{bat}})\, i_{\mathrm{bat}} \quad (16)$$

$$SOC_{\mathrm{bat}} = SOC_{\mathrm{init}} - \frac{1}{3600\, C_{\mathrm{bat}}} \int_0^t i_{\mathrm{bat}}\, dt \quad (17)$$

where u_{bat} is the battery voltage and C_{bat} is the battery capacity (Ah).

b. Transmission: Reduction gearbox & 2-speed gearbox

Unlike the AMT gearbox of the ICE-based HDV, no efficiency maps are used for the transmission part of the EVT-based HDV. The gear ratios of the 2-speed gearbox and the reduction gearboxes are not the same as the ones used in the conventional truck. Therefore, it is assumed that these latter have average efficiencies ($\eta_{\mathrm{gb}}, \eta_{\mathrm{red}}$) of 97% [52]. This assumption is widely used in literature due to the lack of data and accurate scalable efficiency models of gearboxes. In case a reduction gearbox is present between the ICE and the inner rotor, for example, **Topology B** and **C** (see Fig. 6.b and c), the model (18) is used. If no gearbox exists like in **Topology A** (see Fig. 6.a), the model (19) is used.

$$\begin{cases} T_{\mathrm{IR}} = \dfrac{T_{ICE}\, \eta_{\mathrm{red}}^{\mathrm{sign}(\mathrm{T_{ICE}})}}{k_{\mathrm{red}}} \\ \Omega_{\mathrm{IR}} = k_{\mathrm{red}}\, \Omega_{\mathrm{ICE}} \end{cases} \quad (18)$$

$$\begin{cases} T_{\mathrm{ICE}} = T_{\mathrm{IR}} \\ \Omega_{\mathrm{IR}} = \Omega_{\mathrm{ICE}} \end{cases} \quad (19)$$

Similarly, for the 2-speed gearbox, the models (20) and (21) are used according to the topology. Note that the 2-speed gearbox used in Topology C (see Fig. 6.c) can take two ratios, which are going to be defined in Section.4 through an optimization procedure. If no 2-speed gearbox is present as in the cases of **Topology A & B** (see Fig. 6.a), the model (21) is then used. Finally, both of the gearboxes are described by mono-domain conversion elements.

$$\begin{cases} T_{\mathrm{gb}} = k_{\mathrm{gb}}\, T_{\mathrm{OR}}\, \eta_{\mathrm{gb}}^{\mathrm{sign}(\mathrm{T_{OR}})} \\ \Omega_{\mathrm{OR}} = k_{\mathrm{gb}}\, \Omega_{\mathrm{gb}} \end{cases} \quad (20)$$

$$\begin{cases} T_{\mathrm{gb}} = T_{\mathrm{OR}} \\ \Omega_{\mathrm{OR}} = \Omega_{\mathrm{gb}} \end{cases} \quad (21)$$

c. Reference EVT

Given this study focuses only on energetic aspects, a static model of the hybrid excited EVT is adopted, i.e. electrical dynamics are neglected. For more information concerning the EVT dynamic model, the reader is referred to [53]. Herein, the windings of the EVT are modelled as follows:

$$\underline{v_{\mathbf{z}}^{\mathbf{0}}} = \underline{\boldsymbol{R}}\, \underline{i_{\mathbf{z}}^{\mathbf{0}}} - \underline{e_{\mathbf{z}}^{\mathbf{0}}} \quad (22)$$

It should be noted that the subscript **z** refers to the quadratic (q) and direct (d) axes components of park transform for the stator (s), the inner rotor (IR) and outer rotor (OR). This latter can be substituted by $\{\mathrm{s_d}, \mathrm{s_q}, \mathrm{IR_d}, \mathrm{IR_q}, \mathrm{OR_d}\}$. The superscript **0** refers to the reference EVT. $\underline{\boldsymbol{R}}$ is a diagonal matrix (5x5) containing the values of the stator, outer rotor and inner rotors resistances. The electromagnetic torque on both rotors, expressed in a vector $\underline{T_{\mathrm{r}}^{0}} = \begin{bmatrix} T_{\mathrm{IR}}^{0} \\ T_{\mathrm{OR}}^{0} \end{bmatrix}$, are calculated based on eq. (23), in which N_{p} and ψ

are the number of pole pairs and the flux respectively. It is worth noting that the iron losses P_{fer} in both stator and inner rotor are taken into consideration by subtracting a torque related to these losses. Additionally, the losses originated from the bearings and the slip rings are considered, by subtracting a related torque T_{bsr} from the overall torque:

$$\begin{cases} T_{\mathrm{s}}^{0} = N_{\mathrm{p}}\left(\psi_{\mathrm{s_d}} i_{\mathrm{s_q}} - \psi_{\mathrm{s_q}} i_{\mathrm{s_d}}\right) - \dfrac{P_{\mathrm{fer_s}}}{\Omega_{\mathrm{OR}}} \\ T_{\mathrm{IR}}^{0} = N_{\mathrm{p}}\left(\psi_{\mathrm{IR_d}} i_{\mathrm{IR_d}} - \psi_{\mathrm{IR_q}} i_{\mathrm{IR_d}}\right) - \dfrac{P_{\mathrm{fer_{IR}}}}{\Omega_{\mathrm{IR}} - \Omega_{\mathrm{OR}}} - T_{\mathrm{bsr_{IR}}} \\ T_{\mathrm{OR}}^{0} = -T_{\mathrm{s}}^{0} - T_{\mathrm{IR}}^{0} - T_{\mathrm{bsr_{OR}}} \end{cases} \quad (23)$$

Finally, the back-emf $\underline{e_z^0}$ in the stator and inner rotor is calculated according to (24).

$$\underline{e_z^0} = \left[-\Omega_{\mathrm{OR}} N_{\mathrm{p}} \psi_{\mathrm{s_d}} \quad \Omega_{\mathrm{OR}} N_{\mathrm{p}} \psi_{\mathrm{s_q}} \quad 0 \quad -(\Omega_{\mathrm{OR}} - \Omega_{\mathrm{IR}}) N_{\mathrm{p}} \psi_{\mathrm{IR_d}} \quad (\Omega_{\mathrm{OR}} - \Omega_{\mathrm{IR}}) N_{\mathrm{p}} \psi_{\mathrm{IR_q}}\right]^{\mathrm{T}} \quad (24)$$

The main parameters of the reference EVT are summarized in the following table:

Table 3: Reference electrical variable transmission parameters

	Stator	**Outer rotor**	**Inner rotor**
Rated power [kW]	77	120	75
Rated current amplitude [A]	265	4.6 (DC)	150
Continuous torque [Nm]	245	382	137
Number of pole pairs N_{p}		4	
Outer radius r^0[mm]	169	123.5	102
Inner radius [mm]	124.5	103	57
Active axial length l_{a}^0 [mm]	87	87	87
Winding resistance [Ω]	0.0221	12.73	0.0256
Maximum speed [rpm]		6000	6000

d. Scaled EVT using power adaptation elements

To predict the performance of the new EVT design, scaling laws have been applied to the actual EVT prototype design, of which all the parameters are well-known (see Table 3). This scaling methodology has been validated and published in [25]. Such a theory is based on three scaling factors, which are axial (K_{A}), radial (K_{R}) and rewinding (K_{w}). The two first scaling factors, axial (K_{A}) and radial (K_{R}), are related to the geometry of the studied machine. The axial scaling consists of lengthening or shortening the axial core length of the machine. While the radial scaling considers a proportional change of all the cross-section dimensions. Finally, the rewinding scaling factor (K_{w}) is used to adapt the electrical machine voltage to the power supply system. Based on the work presented in [24], Lhomme *et al.* proposed a new model structuring of the scaling laws, aiming to integrate them at system-level using EMR [54]. The last methodology was applied to model a scalable EVT for HEV [47]. This new structuration of the model consists of keeping the model of the reference EVT and scale the power at both electrical and mechanical sides. In [47], the scaled EVT was described by adding two Power

Adaptation elements of EMR-oriented backward (PA- square with a mathematical comparison sign inside) inserted at both sides of the reference EVT (see Fig. 7). On the electrical side, the voltage and current relationships between the reference machine and scaled machine are given by eq. (25).

$$\begin{cases} \underline{v_{\mathrm{c}}^{0}} = \underline{v_{\mathbf{z}}^{0}} = \dfrac{\underline{v_{\mathrm{z}}}}{K_{\mathrm{A}} K_{\mathrm{R}} K_{\mathrm{W}}} - \underline{\mathbf{\Delta_R^0}} \underline{i_{\mathbf{z}}^{0}} \\ \underline{i_{\mathrm{c}}} = \underline{i_{\mathrm{z}}} = \dfrac{K_{\mathrm{R}}}{K_{\mathrm{W}}} \underline{i_{\mathbf{z}}^{0}} \end{cases} \quad (25)$$

As can be seen from eq. (26), an equivalent resistor $\underline{\mathbf{\Delta_R^0}}$, containing the core R_{co}^{0} and end winding R_{ew}^{0} resistance terms, is introduced to find the scaled voltages. Moreover, this equivalent resistor is needed to scale the copper losses of the reference EVT, which have a non-linear behavior during the scaling procedure. The $\underline{\mathbf{\Delta_R^0}}$ term is indeed a diagonal matrix (5x5) and the diagonal terms are given by eq. (26) More information on how these models are derived for a PMSM are available in [49].

$$\Delta_{\mathrm{R,y}}^{0} = R_{\mathrm{co,y}}^{0} \left(\frac{1}{K_{\mathrm{R}}^{2}} - 1 \right) + R_{\mathrm{ew,y}}^{0} \left(\frac{1}{K_{\mathrm{A}} K_{\mathrm{R}}} - 1 \right) \quad (26)$$

Note that the subscript **y** refers to the inner, outer rotors, and stator resistances and can be replaced by $\{\mathrm{s}, \mathrm{IR}, \mathrm{OR}\}$. On the mechanical side, the torque of the reference machine $\underline{T_r^0}$ is scaled according to eq. (27), by a power scaling factor equals to $K_{\mathrm{A}} K_{\mathrm{R}}^{2}$. It is important to emphasize that the speeds of the reference $\underline{\Omega_{\mathrm{r}}^{0}}$ and the scaled EVT $\underline{\Omega_{\mathrm{r}}}$ are identical.

$$\begin{cases} \underline{T_{\mathrm{r}}} = K_{\mathrm{A}} K_{\mathrm{R}}^{2} \, \underline{T_r^0} \\ \underline{\Omega_{\mathrm{r}}^{0}} = \underline{\Omega_{\mathrm{r}}} = \begin{bmatrix} \Omega_{\mathrm{IR}} \\ \Omega_{\mathrm{OR}} \end{bmatrix} \end{cases} \quad (27)$$

e. Converters

Losses in the inverters and the chopper, i.e. conduction and switching losses, are taken into account and modelled as proposed in [55]. For simplicity, the three converters are described by one mono-domain conversion element as illustrated in Fig. 7.

$$i_{\mathrm{tract}} = \frac{\underline{v_c} \, \underline{i_c}^{T} - P_{\mathrm{losses,conv}}}{u_{\mathrm{bat}}} \quad (28)$$

where $\underline{v_c}$, $\underline{i_c}$ and $P_{\mathrm{losses,conv}}$ are respectively the voltages, the currents, and the losses of the two inverters and the chopper.

f. Auxiliaries

For the EVT based HDV, auxiliaries are considered as a source of current i_{aux} defined by eq. (29). An average power P_{aux} is considered as well.

$$i_{aux} = \frac{P_{\mathrm{aux}}}{u_{\mathrm{bat}}} \quad (29)$$

The battery current is then the result i_{bat} of the sum of i_{aux} and the traction current i_{tract}.

$$i_{bat} = i_{\mathrm{tract}} + i_{\mathrm{aux}} \quad (30)$$

4. Bi-level optimization framework

This section is devoted to highlighting the optimization process of the EVT-based HDV. The optimization problem of the plant and its control can be solved using different approaches: sequentially, iteratively, nested, and simultaneously [26,27]. When a strong coupling between the plant and control design exists, only nested and simultaneous methods are proved more promising to guarantee system-level optimality than sequential and iteratively methods [29]. The nested method has previously been used in the context of heavy-duty vehicles optimization to define the optimal design for parallel hybrid-electric trucks [26] and battery-electric trucks [49]. Herein, the nested approach will be applied to optimize the plant design of three EVT based-powertrains and their controls. Thus, it can be ensured that the studied powertrains are compared based on their optimal potential. In the subsequent sections, the powertrain design optimization routine of each topology and its constraints are firstly explained. Then, the control optimization methodology is presented. Note that the powertrain design of the ICE-based HDV is assumed already optimized.

4.1. Optimization framework

The nested method splits the overall optimization problem into two levels, an upper level for plant optimization and a lower level for control optimization. Using this approach, the control design is nested within the plant design, i.e. every evaluation of a plant requires a full optimization of the control design. In the upper level, exhaustive search, also known as the brute force search method, is used. Following this approach, the design space is gridded and for each grid point the fuel cost function will be assessed [56]. This method is mostly used in industry to derive trends in system design for discrete component choices. Next, DP will ensure finding the optimal control for every candidate defined in the outer-loop by the brute force search method. Note that other algorithms can be used, e.g. sequential quadratic programming [57], genetic algorithms [28], particle swarm optimization [58] to handle the upper level of the nested approach. Broadly speaking, there is no universal algorithm to address the optimization of the plant design. According to the optimization function and its constraints, an optimization algorithm may prove to be better than others in terms of computational time [59]. More details on the optimization algorithms can be found in the last reference.

Fig. 8 highlights the relevant components, for each topology, to be investigated during the optimization sizing process. Herein, the EVT scaling laws, the differential ratio, the ICE, and battery sizes will be investigated for **Topology A**. Note that for the other topologies, components such as gearboxes are added to the powertrain configuration. Consequently, the sizing of the gear ratios should be included in the optimization routine. The sizing optimization of **Topology B** takes then into account the same components as **Topology A**, but with the addition of the gear ratio of the reduction gearbox in the optimization process. Finally, the gear ratios of the reduction and 2-speed gearboxes are added to the sizing optimization problem of **Topology C**, however, the ratio of the differential is excluded. This choice was made to reduce the number of optimization problem variables.

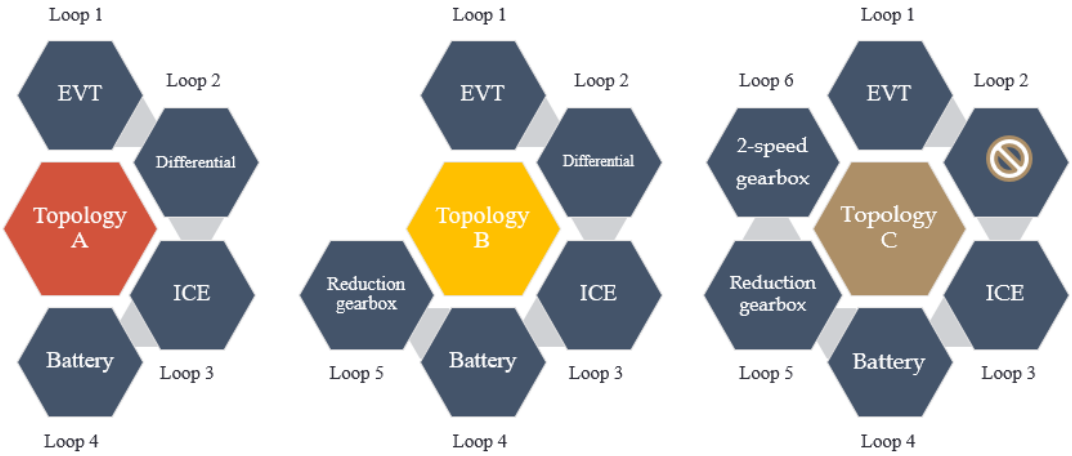

Fig. 8: Component sizing optimization for each topology

All the possible values that these component sizing variables could take are summarised in Table 4 and will be discussed in the sections above. It is emphasized that the upper level contains nested optimization sub-loops devoted to each component (see Fig.9.b). Note that a sub-loop can be skipped in case the chosen topology does not contain the corresponding component (for example loops 5 and 6 are skipped if **Topology A** is used). The main idea here consists of varying one variable at a time and repeating this process until all the sizing variables are explored. The output of the upper level, as illustrated in Fig.9.a, will be a vector x_p containing a candidate combination of the component sizing variables. This vector will be sent to a lower level (the control design optimization). For each candidate set of x_p, DP will ensure finding the corresponding optimal control.

Table 4: Feasible set of powertrain component sizing variables for each topology

Powertrain optimization sub loops	**Sizing**		
	Topology A	**Topology B**	**Topology C**
ICE power (P_{ICE}) [kW]	Common $\boldsymbol{P_{ICE}} \in \{330, 175\}$		
Battery energy E_{bat} [kWh]	Common $\boldsymbol{E_{bat}} \in \{82.5, 41, 20.6\}$		
Scaling factors	$\boldsymbol{T_{OR-max}} = 2200\ N.m$		$\boldsymbol{T_{OR-max}} = 1600\ N.m$
	$\boldsymbol{K_A} \in [0.5,10]$ $\boldsymbol{K_R}$ and $\boldsymbol{K_W}$: see (31) and (32)		
Gear ratio of the ICE reduction gearbox (k_{red})	∅	Variable: $\boldsymbol{k_{red}} \in [2,3]$	
Gear ratio of the differential (k_{diff})	Variable: $\boldsymbol{k_{diff}} \in [10,13]$		Fixed: $\boldsymbol{k_{diff}}$ = 2.63
2-speed gearbox: high gear ratio ($k_{gb-high}$)	∅		Fixed: $\boldsymbol{k_{gb-high}}$ = 5
2-speed gearbox: low gear ratio (k_{gb-low})	∅		Variable: $\boldsymbol{k_{gb-low}} \in [1,4]$

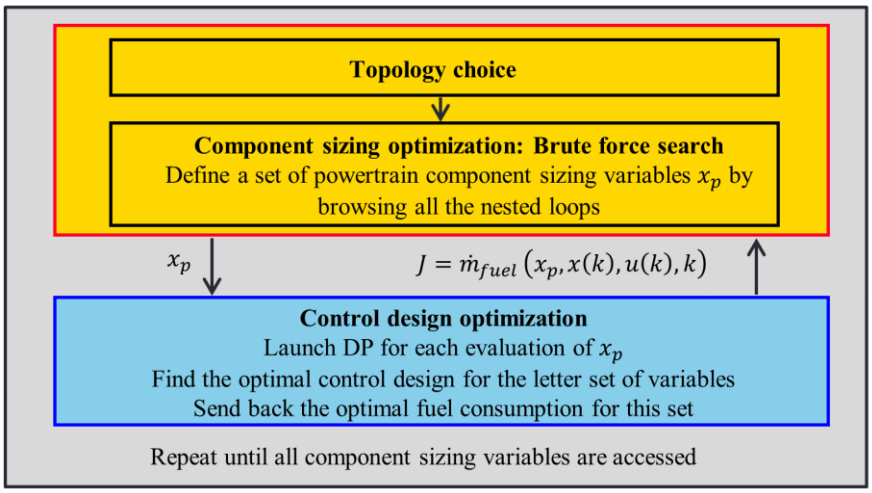

(a)

EVT based HDV- bi-level optimization algorithm

- Define a list with all the feasible sizing values for each component
  Initialization of the iteration counter, i=1
- Browse all the nested loops
  Loop 1: EVT-scaling factor combination (K_A, K_R, K_W)
  Loop 2: ICE reduction gearbox ratio k_{red}
  Loop 3: Differential ratio k_{diff}
  Loop 4: 2-speed gearbox: low gear ratio k_{gb_low}
  Loop 5: Engine power P_{ICE}
  Loop 6: Battery energy E_{bat}
  For each iteration, define a set of the sizing variables x_p
  $x_p(i) = [(K_A, K_R, K_W), k_{red}, k_{diff}, k_{gb\_low}, P_{ICE}, E_{bat}]$
  Launch DP for the defined x_p(i)
  Save the fuel consumption found
  Update the iteration counter, i=i+1
- Repeat until all component sizing variables are browsed

(b)

Fig.9: EVT powertrain co-design optimization:

(a) nested optimization principle, (b) nested-optimization algorithm

4.2. Optimization outer loop: Powertrain sizing optimization

The optimization outer loop requires finding the optimal sizing of each topology. The design optimization and its related constraints for the three topologies are detailed in the following subsections.

a. Topology A

Following Fig. 8, the design optimization loops of **Topology A**, namely the EVT, the differential gear ratio, the ICE, and the battery, are detailed as follows:

Loop 1 - EVT sizing methodology: Sizing and optimizing an electrical machine is a long and complex process, which is based not only on electrical aspects but also on thermal and mechanical considerations. In this study, some simplifications were taken in the EVT sizing process. For instance, the thermal aspects are considered out of scope for this study due to the lack of a scalable thermal model of this EVT version. The new design is herein scaled based on the torque requirements of the studied driving cycle as proposed in [25]. In this case, the EVT outer rotor needs to meet these requirements since it is connected to the final drive. Concerning the EVT of **Topology A**, the reference design is upscaled to

reach a maximum torque of 2200 Nm. This value was found through a backward simulation and corresponds to the long-lasting maximum load point of the driving cycle multiplied by a safety factor. In this way, infeasible solutions due to torque limits, when running the optimization process, can be avoided. The EVT scaling depends on three parameters, which are axial K_{A}, radial K_{R} and rewinding K_{W}. To find the new EVT design, there are an important number of scaling factors combinations. It is important to notice that these factors have a direct impact on the machine losses (e.g. copper and iron losses) [24] and thus the fuel consumption [21]. Therefore, they need to be well chosen. That is why it is decided to integrate these factors in the optimization loops to investigate their impact on fuel consumption. The relation between the axial and radial scaling factors, given a maximum required torque (defined by the considered application), can be found based on the outer rotor force density F_{d} and the geometry parameters of the reference EVT (axial length l_{a}^{0} and radius r^{0}, see Table 3) [25]. Finally, K_{W} is found by dividing the product of K_{A} and K_{R}, to maintain the voltage requirements between the reference and scaled EVT and limit the number of design variables.

$$K_{\mathrm{R}} = \frac{1}{r^{0}} \sqrt{\frac{T_{\mathrm{OR-max}}}{2\,\pi\,F_{\mathrm{d}}\,K_{\mathrm{A}} l_{\mathrm{a}}^{0}}} \qquad (31)$$

$$K_{\mathrm{W}} = \frac{1}{K_{\mathrm{A}}\,K_{\mathrm{R}}} \qquad (32)$$

Loop 2 - Differential: Recall that, the maximum torque of the scaled EVT was obtained through a backward simulation, considering an initial sizing of the differential. To end up with the new EVT size, an initial gear ratio has been set ($k_{\mathrm{diff}} = 10$). A lower ratio could be chosen, but it will lead to a prohibitive sizing of the EVT. This value is then considered as the minimum ratio permissible for the differential sub-loop optimization. The next step consists of investigating the impact of other values for the differential gear ratio on the fuel consumption (see Table 4). Note that the maximum value that the differential gear ratio could take is also subjected to a speed constraint related to the EVT outer rotor maximum speed (6000 rpm, see Table 3).

Loop 3 - ICE: The study will be carried out using two engines. Firstly, the original ICE (324 kW) of the reference vehicle, called big ICE, will be used. Then, this latter will be replaced by a smaller ICE to investigate the fuel savings with a downsized ICE (175 kW). The small ICE has been also extracted from VECTO, so the datasets are comparable in terms of accuracy.

Loop 4 - Battery The impact of the battery size will also be investigated. Herein, the battery size, i.e. the total energy E_{bat}, is changed by modifying the number of battery parallel cells. The number of cells in series was kept fixed to maintain the same voltage for the scaled batteries. For the battery sub-loop optimization, three batteries are considered: a big battery pack of 82.5 kWh, a medium battery pack of 41 kWh, and a small battery pack of 20.6 kWh.

b. Topology B

The same powertrain design optimization routine has been applied for **Topology B**. However, the only difference, in this case, is that a reduction gearbox is added to the optimization problem (loop 5). Herein, the influence of the ICE reduction gearbox gear ratio k_{red} on fuel consumption will be

studied. Since this gearbox is inserted between the ICE and the inner rotor of the EVT, the sizing is subjected to constraints such as the inner rotor maximum speed (6000 rpm, see Table 3) and ICE limitations.

c. Topology C

One of the advantages of adding a 2-speed gearbox to an electrical drivetrain is the possibility to downsize the electrical machine (loop 6). To take this advantage into account, a further case study supposes a downsized EVT for this topology. In this case study, some simplifications were made to simplify the optimization problem and reduce therefore the number of variables to be optimized. That is why it is assumed that the differential gear ratio is the same as the reference truck (k_{diff} = 2.63, see Table 1). As the objective is to downsize the EVT as much as possible, the maximum ratio of the first gear, called high gear $k_{gb-high}$, will play a crucial role. Constraints related to the outer rotor speed (6000 rpm, see Table 3) will define the maximum value of the last-mentioned gear. An EVT design of 1600 Nm is then a result of a maximum value of $k_{gb-high}$. Based on the last assumptions, an EVT design with a maximum torque of less than 1600 Nm will be unfeasible. In the optimization process, the ratio $k_{gb-high}$ will be then fixed to respect the maximum outer rotor torque. It means that only the ratio of the second gear ratio k_{gb-low}, called low gear, will be optimized. For the remaining components, the same optimization routine is considered as the latter topologies. Lastly, it is important to point out that this downsized design and the maximum value of the gear ratios are only valid for the studied driving cycle and could not be generalized to other case studies.

4.3. Optimization inner loop: Control design optimization

At the end of each iteration of the upper level, i.e. powertrain design level, a vector x_p (containing all the component sizing variables detailed above (see Fig.9.a) is defined. For each new candidate set of the powertrain component sizing variables x_p, the control problem (11) need to be solved. As can be seen from Fig. 10, there are two EMS that will manage the power flows in the system. The first EMS, called EMS Truck, will manage the braking strategy via the distribution criteria (k_d), the gear shifting if a gearbox is present through k_{gb} and the ICE setpoints (T^*_{ICE} and Ω^*_{ICE}). This latter EMS will be carried out using DP. Concerning the EMS of the scaled EVT, it will define the optimal current combination set ($\underline{i}_z^{0*}$). In this case, optimizing the current combination (5 currents in the case of this EVT version) of each new design will lead to a cumbersome optimization problem. To tackle this problem, the scalable control theory of PM-EVT has been applied [25]. As shown in Fig. 10.b, optimizing only the control of the reference machine and scale its control is enough. This approach is interesting in system-level optimization problems, to save computational time and to avoid resolving the optimization control of the EVT. In this sense, the EMS of the reference EVT has been optimized based on experimental tests [60]. The results of the optimization routine have been saved in a LUT and

integrated into the DP algorithm of the EMS Truck. This hybrid approach between rules and DP guarantees an optimal solution while reducing the computational time [35].

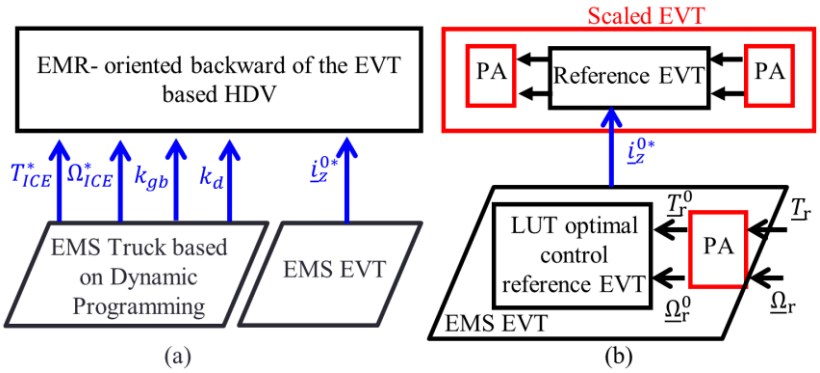

Fig. 10: Identification of the EMS of the EVT based HDV: (a) EMS Truck based on Dynamic Programming (engine operating points, gear shifting and optimal braking) and EMS EVT (b) A focus on the EMS EVT: optimal scaled control of the reference EVT

In this optimization problem, the minimization of the fuel function cost J depends on the combination of the control vector $u(k)$ signals, as depicted in (33). The state variable $x(k)$ in this case is the battery State of Charge (SoC). The constraints related to this variable are the charge sustaining and the depth of discharge. The first constraint requires that the initial and final SoC must be equal. Moreover, the SoC boundaries are limited for battery aging considerations. Here, the SoC is limited between 30% and 70% [61]. Furthermore, other constraints are also considered in the optimization problem. During regenerative braking, the braking distribution criteria k_{d} must be defined in such a way that it would respect the outer rotor maximum torque in generator mode and the maximum battery current charging. Additionally, if a gearbox is used in the topology, the gear shifting strategy must choose the appropriate gear ratio that minimizes the fuel consumption and the losses of the EVT. This has to be done with respect to the outer rotor's maximum speed and torque limitations. Finally, the input setpoints of the ICE must respect its limitation. All these constraints are summarized in eq. (34).

$$u(k) = [T^*_{\mathrm{ICE}}, \Omega^*_{\mathrm{ICE}}, k_{\mathrm{d}}, k_{\mathrm{gb}}]^T \tag{33}$$

$$\begin{cases} SoC(k_0) = SoC(k_{\mathrm{f}}) \\ SoC_{\mathrm{min}} \leq SoC(k) \leq SoC_{\mathrm{max}} \\ i_{\mathrm{bat-min}} \leq i_{\mathrm{bat}}(k) \leq i_{\mathrm{bat-max}} \\ 0 \leq \Omega_{\mathrm{OR}}(k) \leq \Omega_{\mathrm{OR-max}} \\ \mathrm{T}_{\mathrm{OR-min}} \leq \mathrm{T}_{\mathrm{OR}}(k) \leq \mathrm{T}_{\mathrm{OR-max}} \\ 0 \leq T^*_{\mathrm{ICE}}(k) \leq \mathrm{T}_{\mathrm{ICE-max}} \\ \Omega_{\mathrm{ICE-min}} \leq \Omega^*_{\mathrm{ICE}}(k) \leq \Omega_{\mathrm{ICE-max}} \\ 0 \leq \mathrm{k_d}(k) \leq 1 \end{cases} \tag{34}$$

5. Results and Discussion

This section presents the findings of the co-design optimization routine of the EVT-based HDV. Firstly, the results of optimal powertrain sizing, for each topology, are discussed. Subsequently, the influence of each component sizing on the fuel consumption is separately addressed in the remainder of this section.

5.1. Optimal powertrain sizing

This subsection summarizes the findings of the bi-level optimization for each topology. The results are illustrated in Table 5. Before starting the comparison of the studied topologies, a validation step is needed to check whether the constraints imposed in eq. (34) are respected. Firstly, the constraint to sustain the SoC is respected for all topologies (Fig. 11.a). Then, the speed and torque limitations of the outer rotor of the **Topology C** are respected (Fig. 11.b & c). Concerning the ICE operating points, DP managed to choose these setpoints in such a manner as to minimize the global fuel consumption for each topology. As seen from Fig. 11.d, there are some points with a higher BSFC. This is due to the charge sustaining constraint at the end of the driving cycle wherein low torque and speed are needed to have a final SoC equal to the initial one.

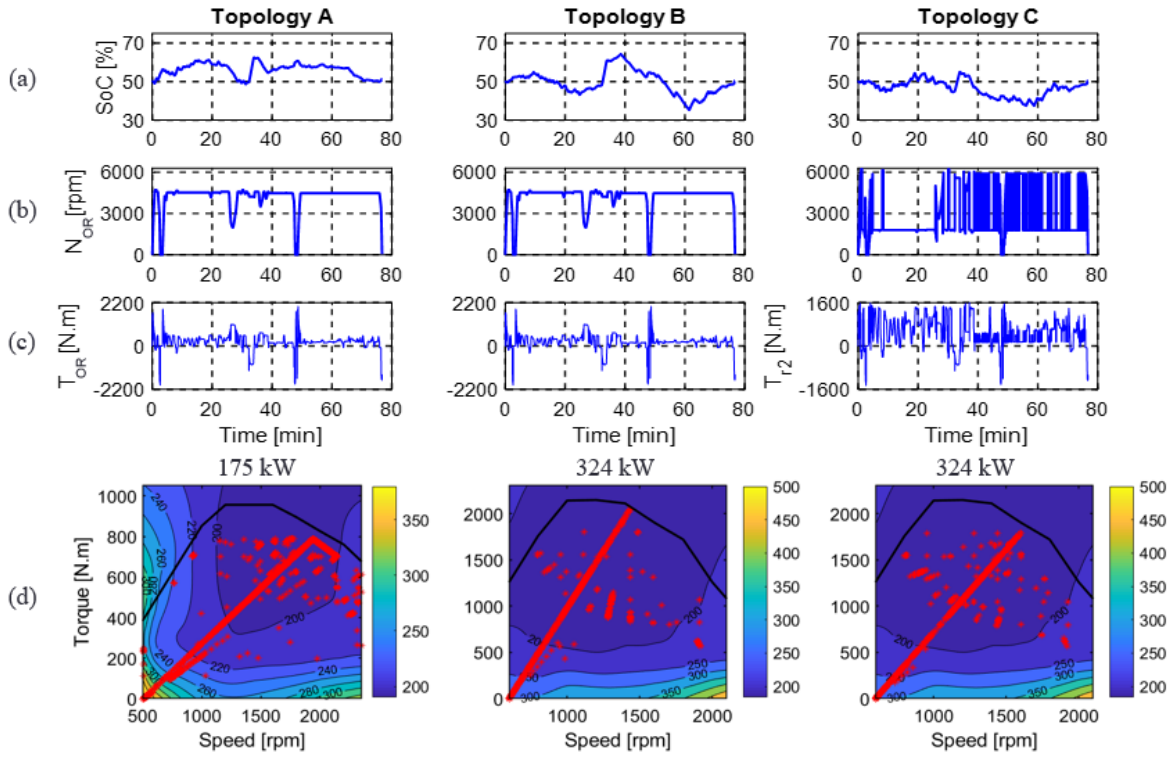

Fig. 11: Constraints validation for all topologies: (a) Battery State of Charge; (b): EVT outer rotor speed; (c): EVT outer rotor torque; (d): Brake specific fuel consumption [g/kWh] of the engine operations points

The optimization revealed that the fuel consumption of **Topology A** is greater than the benchmark, which results in a negative gain (see Fig. 12). This rise in fuel consumption can be explained by two major reasons. First, the inner rotor torque will be high, without a reduction gearbox inserted after the ICE, causing elevated copper losses in the EVT (see Fig.13). Additionally, speed will be low which leads to a high-speed difference between the inner rotor and outer rotor. This results in high iron losses. The fuel gains obtained with **Topology B** and **C**, which use a reduction gearbox for the ICE, confirm the last statements. Furthermore, unlike **Topology B** and **C**, the small ICE is chosen for **Topology A**. This choice made by the optimization algorithm is a trade-off between the engine size and the used

operating range due to the torque limitation of the inner rotor. Henceforth, **Topology A** is considered out of the competition, comparing to the other topology candidates. Finally, **Topology C** presents the best fuel gain. This can be explained by the benefits of the 2-speed gearbox. Thanks to an extra degree of freedom, the average efficiency, during the studied driving cycle, of the EVT is improved compared to the other topologies (see Table 5), resulting in a better fuel gain. Furthermore, it is found that CO_2 emissions are reduced proportionally to fuel economy. This is because the model used in VECTO (8) considers a linear relationship between the emissions and the mass of fuel consumed during the driving cycle.

Table 5: Bi-level optimization findings

Optimization outcomes	**Topology A**	**Topology B**	**Topology C**
ICE power (P_{ICE}) [kW]	Small ICE (175 kW)	Big ICE (324 kW)	Big ICE (324 kW)
Battery energy E_{bat} [kWh]	Big battery (82.5 kWh)	Big battery (82.5 kWh)	Big battery (82.5 kWh)
Scaling factors	$K_A = 1.3$ $K_R = 2.1$ $K_w = 0.366$	$K_A = 1.3$ $K_R = 2.1$ $K_w = 0.366$	$K_A = 1$ $K_R = 2.04$ $K_w = 0.489$
Gear ratio of the ICE reduction gearbox (k_{red})	∅	3	3
Gear ratio of the differential (k_{diff})	10	10	2.63
2-speed gearbox: low gear ratio (k_{gb-low})	∅	∅	1.5
Fuel Gain [%]	**-1.5**	**+12**	**+14.23**
CO_2 emissions reduction [%]	**+1.5**	**-12**	**-14.23**
Average EVT efficiency including converters [%]	**81.8**	**87.6**	**93.64**
Computational time [h]	**4.8**	**7.19**	**12.3**

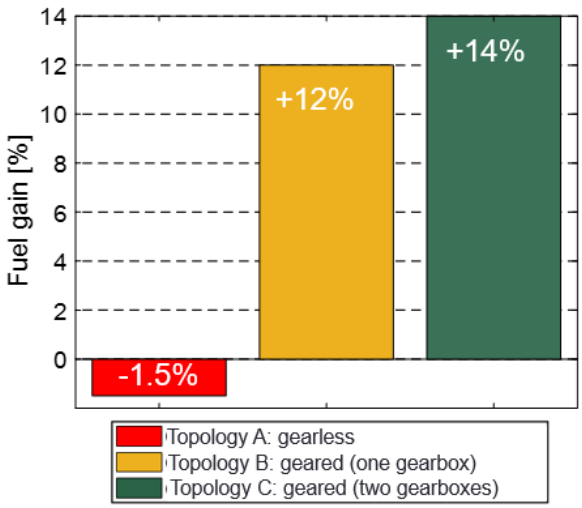

Fig. 12: Fuel savings of optimal powertrain designs of the three studied topologies, determined based on the consumption of the reference truck

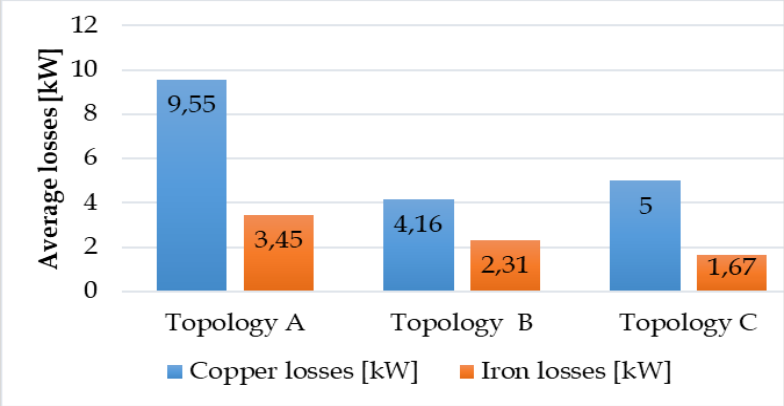

Fig.13: Losses in the EVT of each topology

The computational time needed to solve the optimization problem is reported in Table 5. As it can be seen, the computational burden is important. This is mainly due to the choice of the brute force search method that handled the optimization of the plant design. All possible candidates are evaluated for a given topology, which makes this method time-consuming particularly when the number of design variables increases. This can be seen in the case of **Topology C** where the number of design variables is greater than the other topologies. It is noteworthy to mention that the computational time is not considered as a constraint for the optimization routine and reducing it is not the goal of this paper. On the other hand, one of the advantages of the brute force search method is that all the defined sizing variables are explored. Hence, many combinations are possible and it will be challenging to simultaneously visualize all the sizing variables. For the sake of clarity, it is decided to study the influence of these variables (e.g. EVT scaling factors, gear ratios, energy sources sizing) one at a time by varying one parameter and choosing the optimal sizing for the remaining parameters.

5.2. Effect of the ICE reduction gearbox sizing

For **Topology B** & **C**, the influence of the gear ratio of the single-stage gearbox is studied using both engines. From Fig.14, it is clear that a better fuel gain is obtained with a higher gear ratio whatever the size of the ICE. This is due to the losses in the EVT, as mentioned in the section above. A bigger ratio will decrease the torque, resulting in fewer copper losses in the inner rotor. Moreover, it will decrease the speed difference between outer and inner rotors, which results in fewer iron losses in the stator. The optimization results show that the size of the gear ratio has a moderate impact on the **Topology B**. A maximum gain of 1.3% is obtained with the big ICE and 0.3% with the small one. On the other hand, the gear ratio sizing is impactful when it comes to **Topology C**, as can be seen in Fig.14. The fuel gain is improved by 10.2% compared to the results with the small ratio. This is due to the speed difference between both rotors due to the additional gearbox connected to the ICE.

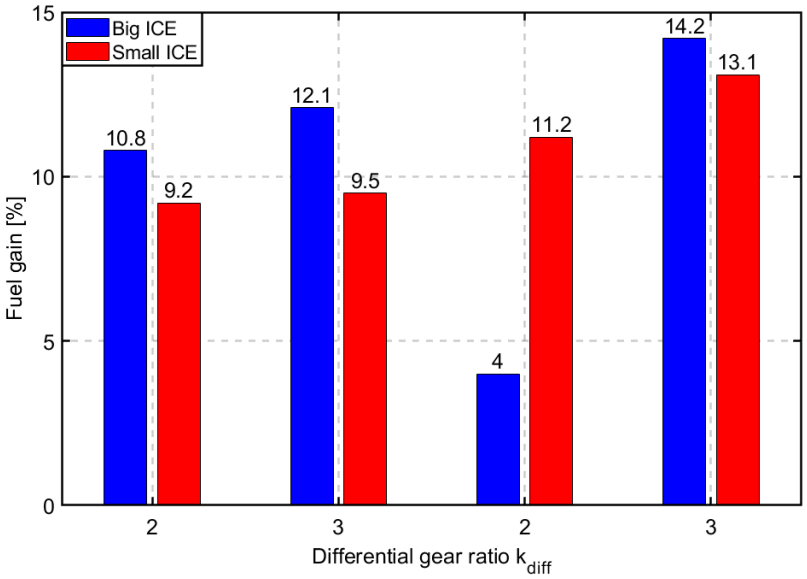

Fig.14: Influence of the reduction gearbox sizing on the fuel gain, as a function of gear ratio and ICE size: calculated based on the consumption of the reference truck.

5.3. Effect of the differential ratio sizing

The optimization process of **Topology B** showed that the differential ratio has no important influence on the fuel consumption in case all other sizing variables are optimal. Indeed, the difference of fuel gain obtained with the optimal and the "worst" ratio is very close (1.1%, see Fig. 15). However, if the latter ratio is combined with an inappropriate ratio of the ICE gearbox, the fuel consumption will increase. Such a case is depicted in Fig. 16 for the **Topology B**. The green marker (at the bottom right corner of Fig. 16) shows that the fuel gain will be less than 8% if the choice of these ratios is poorly defined, which results in decreasing the optimal gain by around 4% compared to the optimal combination (red marker at the top left corner of Fig. 16).

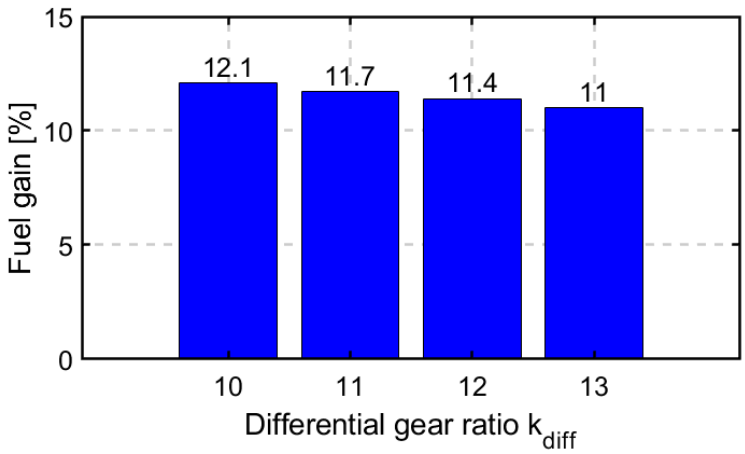

*Fig. 15: Influence of the differential ratio sizing k_{diff} - **Topology B***

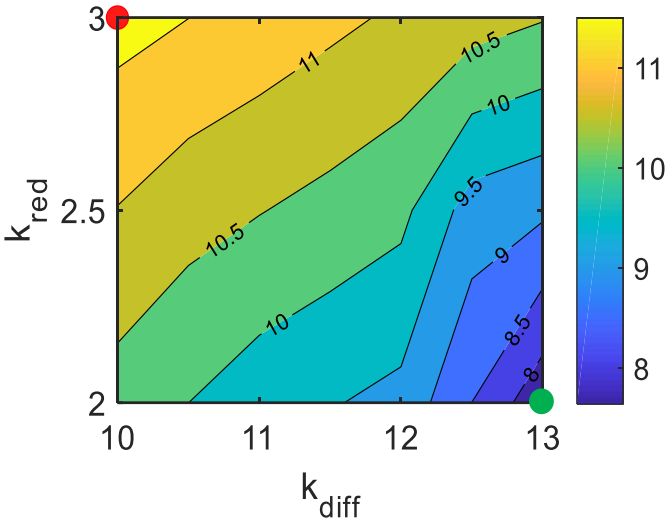

Fig. 16: Influence of the transmission ratios sizing: fuel gain (in percent) as a function of the differential ratio k_{diff} and the single stage gearbox k_{red}- ***Topology B***

5.4. Effect of the scaling factors sizing

Considering an optimal sizing for the remaining component, the influence of the scaling factors of the EVT is illustrated for **Topology B** in Fig. 17. The fuel gain is shown as a function of axial and radial scaling factors. For good accuracy, the axial scaling factors was varied from 0.5 to 10. The radial and rewinding factors were determined according to (31) and (32). This figure allows finding the optimal design, which is defined by $K_{\mathrm{A}} = 1.3$ and $K_{\mathrm{R}} = 2.1$ (marked in red). Moreover, from this figure, it can be seen that the difference between the fuel gains for various EVT designs is small. For example, the difference between a long and a short design in terms of fuel savings is less than 1.5%. This finding is important in case constraints related to the volume or the dimensions will be imposed on the optimization.

5.5. Effect of the 2-speed gearbox gear ratio sizing

From Fig. 18, it can be deduced that the sizing of the low gearbox ratio has an important impact on the fuel consumption of **Topology C**. Here, optimal fuel consumption is obtained with a ratio of 1.5 (marked in red at the top left). The figure indicates that the difference between the optimum and the lowest fuel gain is about 6%, which demonstrates the importance of the optimization process for this variable. As mentioned previously, an inadequate combination with other parameters such as the gear ratio of the ICE gearbox can lead to unsatisfactory results. For instance, the green marker (bottom right corner) in Fig. 18 indicates a negative gain, which means that the fuel consumption with the chosen combination is superior to the reference truck.

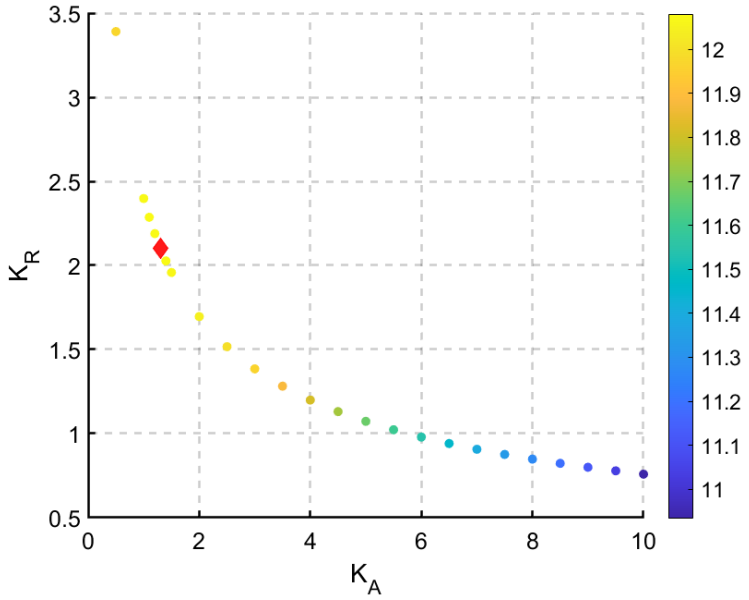

Fig. 17: Influence of the EVT designs: fuel gain (in percent) as a function of axial K_A and radial K_R scaling factor - ***Topology B***

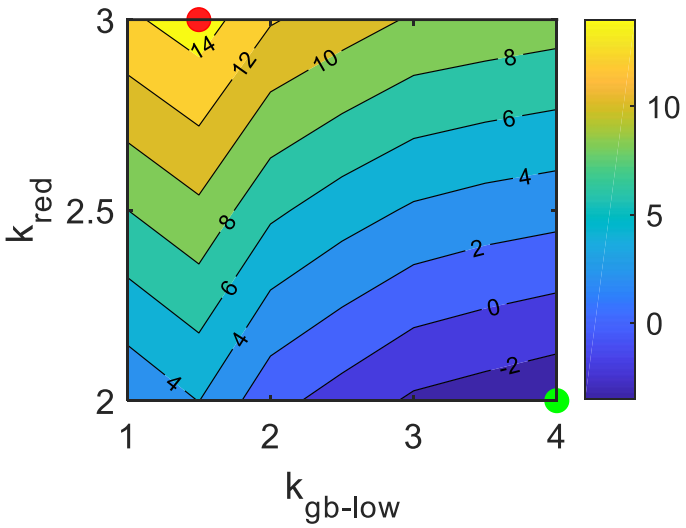

*Fig. 18: Influence of the transmission gear ratios sizing: fuel gain (in percent) as a function of the single-stage gearbox k_{red} and the low gear ratio $k_{\mathrm{gb-low}}$ of the 2-speed gearbox -**Topology C***

5.6. Effect of the energy sources sizing

Note that choosing the best combination of energy sources sizing depends on the objective of the study. Herein, the study focuses only on fuel consumption. According to Fig. 19, the optimal fuel economy is obtained with a big ICE and a big battery. The results revealed that the size of the ICE has a slight impact on fuel savings. Indeed, the difference of the fuel economy between the big and the small ICE varies between 0.7% and 2.6% for all battery sizes, considering **Topology B** and **C**. Therefore, this finding shows that it is possible to roughly achieve similar fuel gains with a small ICE. As a result, the component cost of the powertrain can be reduced. On the other hand, the battery sizing is very impactful, as there is a huge difference in fuel gains between the three considered batteries. From Fig. 19 the

difference in fuel gain between big and medium batteries is moderate (from 0.5% to 1.4%). However, the fuel savings in the case of big and small batteries are quite significant. For example, the fuel gain decreased by 5.5% and 10.9% in the case of **Topology B** and **C** respectively. This can be explained by the total recovered energy during braking, which will be more important in the case of a bigger battery. Unlike big and medium batteries, the upper SoC boundary has been changed to 90% for the small battery to achieve feasible solutions. Otherwise, infeasibility issues will occur, considering an interval of SoC between 30% and 70%. This is mainly due to a smaller battery capacity and lower charge and discharge currents, which has led to the use of a higher SoC range to get feasible solutions for the control problem. Nevertheless, a high SoC could have an impact on battery aging. Note that battery aging is not considered and is out of the scope of this paper. For further analysis of the best sizing of both battery and ICE, it is recommended to reinforce these findings by investigating battery aging and analyzing the total cost of ownership.

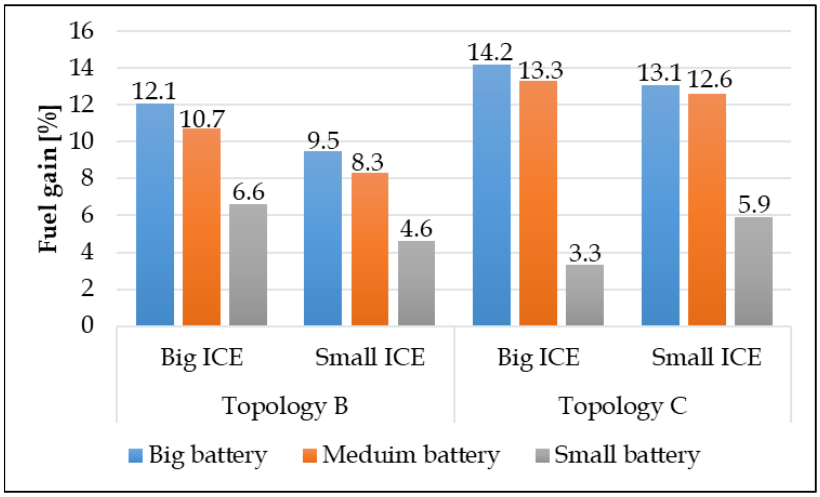

Fig. 19: Influence of the energy sources sizing

Finally, the following table summarizes the impact of each component sizing on fuel consumption.

Table 6: Impact of each component sizing on fuel consumption

Component	Impact on fuel consumption
ICE reduction gearbox	High
2-speed gearbox	High
Differential	Low
Scaling factors	Low
ICE	Moderate
Battery	High

6. Conclusion

In this paper, a conventional long-haul heavy-duty vehicle has been hybridized using a hybrid excited Electrical Variable Transmission (EVT). The main objective of this work was to investigate the potential of such transmission in terms of fuel savings. To this end, three different topologies of a hybrid

EVT powertrain, have been investigated. To ensure that the studied powertrains are compared based on their optimal potential, a bi-level optimization framework has been considered. A nested approach, which incorporates the optimization of the powertrain sizing (brute force search method) and control design (dynamic programming), has been used. The optimization routine results showed a reduction of the fuel consumption from 3.3% to 14.2% for the geared topologies. This results in a reduction in CO_2 emissions in the same proportions. The sizing of these topologies has shown that better fuel savings can be achieved, if all the components are optimally sized based on their interaction. These findings are important, considering a long-haul truck and the studied driving cycle, which is dominated by low dynamics and a constant speed. The fuel savings may be greater in the case of a regional delivery mission, which is characterized by a more dynamic speed profile. Moreover, the optimization routine has revealed the importance of considering all the levels of the system-level design in the optimization problem (architecture, size, etc...) and their interactions. A poorly defined architecture or sizing can lead to unsatisfactory results and not reveal the true potential of a new component under testing. This is the case of the gearless topology, which had led to a fuel consumption greater than the fuel benchmark of the engine-powered truck.

Future research should consider adding further topologies and including the total cost of ownership for the studied cases to take into account the economic impact of the comparison. Furthermore, the powertrain sizing algorithm needs to be changed. In the case of many variables, the brute force search method is very consuming in terms of computational effort. Other algorithms such as a genetic algorithm or particle swarm optimization could be employed.

CRediT authorship contribution statement

Ayoub Aroua: Conceptualization, Methodology, Software, Formal analysis, Visualization, Writing - Original Draft, Writing - Review & Editing. **Walter Lhomme**: Supervision, Funding acquisition, Methodology, Software, Writing - Review & Editing. **Eduardo Redondo-Iglesias**: Resources, Writing - Review & Editing. **Florian Verbelen**: Supervision, Methodology, Software, Writing - Review & Editing.

Declaration of competing interest

The authors declare that they have no known competing financial interests or personal relationships that could have appeared to influence the work reported in this paper.

Acknowledgments

This work has been done within the EVOLUTION (EffectiVeness Of Lorries and bUses using innovative TransmissION) project. EVOLUTION is a collaborative project between the University of Lille and Ghent University. This study was supported by the French government through the Programme Investissement d'Avenir (I-SITE ULNE / ANR- 16-IDEX-0004 ULNE) managed by the Agence

Nationale de la Recherche. Additionally, this work has been achieved within the framework of CE2I project (Intelligent Integrated Energy Converter). CE2I is co-financed by European Union with the financial support of the European Regional Development Fund (ERDF), French State, and the French Region of Hauts-de-France.

References

[1] Muncrief, R., & Sharpe, B. (2015). Overview of the heavy-duty vehicle market and CO2 emissions in the European Union. *International Council on Clean Transportation*.

[2] Official Journal of the European Union. (2019). Regulation (EU) 2019/ of the European Parliament and of the Council of 20 June 2019 setting CO2 emission performance standards for new heavy-duty vehicles and amending Regulations (EC) No 595/2009 and (EU) 2018/956 of the European Parliament and of the Council and Council Directive 96/53/EC.

[3] Delgado, O., & Gonzalez, F. (2018). CO_2 Emissions and Fuel Consumption Standards for Heavy-Duty Vehicles in the European Union. *International Council on Clean Transportation.*

[4] Nikiforos, Z., & Gerogios, F. (2016). Report on VECTO technology simulation capabilities and future outlook. Publications Office of the European Union.

[5] Fontaras, G., Grigoratos, T., Savvidis, D., Anagnostopoulos, K., Luz, R., Rexeis, M., & Hausberger, S. (2016). An experimental evaluation of the methodology proposed for the monitoring and certification of CO2 emissions from heavy-duty vehicles in Europe. Energy, 102, 354-364.

[6] Mulholland, E., Teter, J., Cazzola, P., McDonald, Z., & Gallachóir, B. P. Ó. (2018). The long haul towards decarbonising road freight–A global assessment to 2050. Applied energy, 216, 678-693

[7] Delgado, O., Rodríguez, F., & Muncrief, R. (2017). Fuel efficiency technology in european heavy-duty vehicles: Baseline and potential for the 2020–2030 time frame. communications, 49(30), 847129-102.

[8] Ehsani, M., Gao, Y., Longo, S., & Ebrahimi, K. (2018). Modern electric, hybrid electric, and fuel cell vehicles. CRC press.

[9] Hayes, J. G., & Goodarzi, G. A. (2018). Electric powertrain: Energy systems, power electronics and drives for hybrid, electric and fuel cell vehicles. John Wiley & Sons

[10] Kim, D. M., Benoliel, P., Kim, D. K., Lee, T. H., Park, J. W., & Hong, J. P. (2019). Framework development of series hybrid powertrain design for heavy-duty vehicle considering driving conditions. IEEE Transactions on Vehicular Technology, 68(7), 6468-6480.

[11] Rodríguez, F., & Delgado, O. (2019). The Future of VECTO: CO_2 Certification of Advanced Heavy-Duty Vehicles in the European Union

[12] Holmes, A. G., & Schmidt, M. R. (2002). Hybrid Electric. Powertrain Including a Two-mode Electrically. Variable Transmission .U.S. Patent No. 6,478,705. Washington, DC: U.S. Patent and Trademark Office.

[13] Huang, K., Xiang, C., Ma, Y., Wang, W., & Langari, R. (2017). Mode shift control for a hybrid heavy-duty vehicle with power-split transmission. *Energies, 10(2), 177*.

[14] Zhuang, W., Zhang, X., Ding, Y., Wang, L., & Hu, X. (2016). Comparison of multi-mode hybrid powertrains with multiple planetary gears. *Applied energy, 178, 624-632*.

[15] Lhomme, W., Bouscayrol, A., Syed, S. A., Roy, S., Gailly, F., & Pape, O. (2017). Energy savings of a hybrid truck using a Ravigneaux gear train. IEEE Transactions on Vehicular Technology, 66(10), 8682-8692.

[16] Hoeijmakers, M. J., & Ferreira, J. A. (2006). The electric variable transmission. IEEE Transactions on Industry Applications, 42(4), 1092-1100.

[17] Cheng, Y., Trigui, R., Espanet, C., Bouscayrol, A., & Cui, S. (2011). Specifications and design of a PM electric variable transmission for Toyota Prius II. *IEEE Transactions on Vehicular Technology*, *60*(9), 4106-4114.

[18] Pisek, P., Stumberger, B., Marcic, T., & Virtic, P. (2012). Design analysis and experimental validation of a double rotor synchronous PM machine used for HEV. *IEEE Transactions on Magnetics, 49(1), 152-155.*

[19] Druant, J., Vansompel, H., De Belie, F., Melkebeek, J., & Sergeant, P. (2016). Torque analysis on a double rotor electrical variable transmission with hybrid excitation. *IEEE Transactions on Industrial Electronics, 64(1), 60-68.*

[20] Druant, J., Vansompel, H., De Belie, F., & Sergeant, P. (2017). Loss identification in a double rotor electrical variable transmission. IEEE Transactions on Industrial Electronics, 64(10), 7731-7740.

[21] Verbelen, F., Lhomme, W., Vinot, E., Stuyts, J., Vafaeipour, M., Hegazy, O., & Sergeant, P. (2020). Comparison of an optimized electrical variable transmission with the Toyota Hybrid System. Applied Energy, 278, 115616.

[22] Ma, Z., Lhomme, W., & Bouscayrol, A. (2019, October). Comparison of Gearless Hybrid Transmissions for a Medium-Duty Truck. In 2019 IEEE Vehicle Power and Propulsion Conference (VPPC) (pp. 1-6).

[23] Johannesson, L., Pettersson, S., & Egardt, B. (2009). Predictive energy management of a 4QT series-parallel hybrid electric bus. *Control Engineering Practice*, *17*(12), 1440-1453.
[24] Stipetic, S., Zarko, D., & Popescu, M. (2016). Ultra-fast axial and radial scaling of synchronous permanent magnet machines. *IET Electric Power Applications, 10(7), 658-666.*
[25] Verbelen, F., Abdallh, A., Vansompel, H., Stockman, K., & Sergeant, P. (2020). Sizing Methodology Based on Scaling Laws for a Permanent Magnet Electrical Variable Transmission. *IEEE Transactions on Industrial Electronics, 67(3), 1739-1749*
[26] Silvas, E. (2015). Integrated optimal design for hybrid electric vehicles. Ph.D. dissertation, Eindhoven University of Technology.
[27] Silvas, E., Hofman, T., Murgovski, N., Etman, L. P., & Steinbuch, M. (2016). Review of optimization strategies for system-level design in hybrid electric vehicles. *IEEE Transactions on Vehicular Technology, 66(1), 57-70.*
[28] Kabalan, B., Vinot, E., Yuan, C., Trigui, R., Dumand, C., & El Hajji, T. (2019). Efficiency Improvement of a Series–Parallel Hybrid Electric Powertrain by Topology Modification. *IEEE Transactions on Vehicular Technology, 68(12), 11523-11531.*
[29] Fathy, H. K., Reyer, J. A., Papalambros, P. Y., & Ulsov, A. G. (2001). On the coupling between the plant and controller optimization problems. *In Proceedings of the 2001 American Control Conference.(Cat. No. 01CH37148) (Vol. 3, pp. 1864-1869).*
[30] Vinot, E., Trigui, R., Cheng, Y., Espanet, C., Bouscayrol, A., & Reinbold, V. (2013). Improvement of an EVT-based HEV using dynamic programming. *IEEE Transactions on Vehicular Technology*, *63*(1), 40-50.
[31] Sundström, O., Ambühl, D., & Guzzella, L. (2010). On implementation of dynamic programming for optimal control problems with final state constraints. *Oil & Gas Science and Technology–Revue de l'Institut Français du Pétrole, 65(1), 91-102*
[32] Ma, Z., Murgovski, N., Egardt, B., & Cui, S. (2019). Comprehensive Analysis and Optimal Configurations of the EVT Powertrain. *IEEE Transactions on Vehicular Technology, 68(10), 9573-9587.*
[33] Rodríguez, F. (2018). The European Commission's proposed CO2 standards for heavy-duty vehicle. *International Council on Clean Transportation White Pap*
[34] European Commission staff working document impact assessment. (2018). Proposal for a Regulation of the European Parliament and of the Council setting CO2 emission performance standards for new heavy duty vehicles.
[35] Horrein, L., & Bouscayrol, A. (2019). Model Reduction Methodology for Energy Management Strategy of Hybrid Electric Vehicles. *In 2019 IEEE Vehicle Power and Propulsion Conference (VPPC) (pp. 1-6).*
[36] Bouscayrol, A., Hautier, J. P., & Lemaire‐Semail, B. (2012). Graphic formalisms for the control of multi‐physical energetic systems: COG and EMR. Systemic design methodologies for electrical energy systems: analysis, synthesis and management, 89-124.
[37] Boulon, L., Bouscayrol, A., Hissel, D., Pape, O., & Pera, M. C. (2012). Inversion-based control of a highly redundant military HEV. *IEEE transactions on Vehicular Technology, 62(2), 500-510*
[38] Castaings, A., Lhomme, W., Trigui, R., & Bouscayrol, A. (2016). Comparison of energy management strategies of a battery/supercapacitors system for electric vehicle under real-time constraints. *Applied Energy, 163, 190-200.*
[39] Mayet, C., Welles, J., Bouscayrol, A., Hofman, T., & Lemaire-Semail, B. (2019). Influence of a CVT on the fuel consumption of a parallel medium-duty electric hybrid truck. *Mathematics and Computers in Simulation, 158, 120-129.*
[40] Letrouvé, T., Bouscayrol, A., & Lhomme, W. (2009). Influence of the clutch model in a simulation of a parallel Hybrid Electric Vehicle. *In 2009 IEEE Vehicle Power and Propulsion Conference (pp. 1330-1337).*
[41] Vehicle Energy Consumption Calculation Tool (VECTO), version 3.3, User Manual, in simulation models, fuel proprieties section.
[42] Franco, V., Delgado, O., & Muncrief, R. (2015). Heavy-duty vehicle fuel-efficiency simulation: A comparison of US and EU tools. *International Council on Clean Transportation, Washington, DC.*
[43] Guzzella, L., & Sciarretta, A. (2013). Electric and hybrid-electric propulsion systems. In Vehicle Propulsion Systems (pp. 67-162). Springer, Berlin, Heidelberg.
[44] Ngo, D. V., Hofman, T., Steinbuch, M., Serrarens, A., & Merkx, L. (2010). Improvement of fuel economy in Power-Shift Automated Manual Transmission through shift strategy optimization-an experimental study. *In 2010 IEEE Vehicle Power and Propulsion Conference (pp. 1-5).*
[45] Xu, C., Al-Mamun, A., Geyer, S., & Fathy, H. K. (2018). A dynamic programming-based real-time predictive optimal gear shift strategy for conventional heavy-duty vehicles. *In 2018 Annual American Control Conference (ACC) (pp. 5528-5535).*
[46] Vinot, E., Reinbold, V., & Trigui, R. (2015). Global optimized design of an electric variable transmission for HEVs. *IEEE Transactions on Vehicular Technology, 65(8), 6794-6798.*

[47] Verbelen, F., Lhomme, W., Aroua, A., Bouscayrol, A., & Sergeant, P. (2020) Scalable Electrical Variable Transmission model for HEV simulations using Energetic Macroscopic Representation. *IEEE Vehicle Power and Propulsion Conference*.
[48] Verbruggen, F. J., Rangarajan, V., & Hofman, T. (2019, July). Powertrain design optimization for a battery electric heavy-duty truck. *In 2019 American Control Conference (ACC) (pp. 1488-1493)*. IEEE
[49] Verbruggen, F. J., Silvas, E., & Hofman, T. (2020). Electric Powertrain Topology Analysis and Design for Heavy-Duty Trucks. *Energies, 13(10), 2434*
[50] Castaings, A. (2016). Energy management of multi-source electric and hybrid vehicles using the Energetic Macroscopic Representation. Ph.D. dissertation (text in French), University of Lille.
[51] Einhorn, M., Conte, F. V., Kral, C., & Fleig, J. (2012). Comparison, selection, and parameterization of electrical battery models for automotive applications. *IEEE Transactions on Power Electronics, 28(3), 1429-1437*.
[52] Naunheimer, H., Bertsche, B., Ryborz, J., & Novak, W. (2011). Automotive Transmissions: fundamentals, selection, design and application. Springer Berlin Heidelberg. https://doi.org/10.1007/978-3-642-16214-5.
[53] Druant, J. (2018). Modeling and Control of an Electrical Variable Transmission with Hybrid Excitation, Ph.D. dissertation, Ghent University.
[54] Lhomme, W., Verbelen, F., Ibrahim, M. N., & Stockman, K. (2020). Energetic Macroscopic Representation of Scalable PMSM for Electric Vehicles. *IEEE Vehicle Power and Propulsion Conference*. IEEE.
[55] Wintrich, A., Nicolai, U., Tursky, W., & Reimann, T. (2011). Application manual power semiconductors. Semikron international GmbH. ed: ISLE Verlag, Illmenau.
[56] Cormen, T. H., Leiserson, C. E., Rivest, R. L., & Stein, C. (2009). Introduction to algorithms. MIT press.
[57] D.-G. Li, Y. Zou, X.-S. Hu, and F.-C Sun. Optimal sizing and control strategy design for heavy hybrid electric truck. *In Vehicle Power and Propulsion Conference (VPPC), 2012 IEEE, pages 1100–1106, 2012*
[58] Altan, A. (2020, October). Performance of metaheuristic optimization algorithms based on swarm intelligence in attitude and altitude control of unmanned aerial vehicle for path following. *In 2020 4th International Symposium on Multidisciplinary Studies and Innovative Technologies (ISMSIT) (pp. 1-6)*.
[59] Silvas, E., Bergshoeff, E., Hofman, T., & Steinbuch, M. (2014, October). Comparison of bi-level optimization frameworks for sizing and control of a hybrid electric vehicle. In *2014 IEEE Vehicle Power and Propulsion Conference (VPPC)* (pp. 1-6).
[60] Druant, J., Vansompel, H., De Belie, F., & Sergeant, P. (2017). Optimal control for a hybrid excited dual mechanical port electric machine. *IEEE Transactions on Energy Conversion, 32(2), 599-607*.
[61] Gao, Y., Jiang, J., Zhang, C., Zhang, W., & Jiang, Y. (2018). Aging mechanisms under different state-of-charge ranges and the multi-indicators system of state-of-health for lithium-ion battery with Li (NiMnCo) O2 cathode. *Journal of Power Sources, 400, 641-651*.